

UNIVERSITY OF CALIFORNIA

Los Angeles

**Impact of the Southern Annular Mode on
Southern Ocean Circulation and
Biogeochemistry**

A dissertation submitted in partial satisfaction of the
requirements for the degree Doctor of Philosophy
in Atmospheric Sciences

by

Nicole Suzanne Lovenduski

2007

The dissertation of Nicole Suzanne Lovenduski is approved.

Alexander Dean Hall

Rebecca Fe Shipe

J. David Neelin

James C. McWilliams, Committee Co-chair

Nicolas Gruber, Committee Co-chair

University of California, Los Angeles

2007

Contents

1	Introduction	1
2	Impact of the Southern Annular Mode on Southern Ocean circulation and biology	8
2.1	Abstract	8
2.2	Introduction	9
2.3	Data sources and analysis	10
2.4	Results and discussion	11
2.5	Impact on carbon cycle	17
2.6	Conclusions	18
3	Large scale patterns of variability in the Southern Ocean	19
3.1	Abstract	19
3.2	Introduction	20
3.3	Methods	23
3.4	Modes of variability	25
3.5	Causes of the variability	27
3.6	Discussion	32
3.7	Conclusions	35
4	Enhanced CO₂ outgassing in the Southern Ocean from a positive phase of the Southern Annular Mode	37
4.1	Abstract	37
4.2	Introduction	38
4.3	Methods	44

4.4	Model evaluation	49
4.5	Variability of air-sea CO ₂ fluxes	54
4.6	Causes of the variability	58
4.7	Trends in air-sea CO ₂ fluxes	66
4.8	Summary	67
5	Long-term trends in the Southern Ocean carbon sink	70
5.1	Abstract	70
5.2	Introduction	71
5.3	Methods	72
5.4	Trends in air-sea CO ₂ fluxes	74
5.5	Causes of the trends	75
5.5.1	Natural CO ₂	75
5.5.2	Anthropogenic CO ₂	81
5.6	Implications for the future	83
5.7	Conclusions	84
6	Summary and conclusions	86
A	<i>p</i>CO₂ calculations	91
B	Biological fluxes	93

List of Figures

1.1	Mean wind speed, SST, and sea ice.	2
1.2	The Antarctic Circumpolar Current and the Deacon Cell.	3
1.3	Mean nitrate and chlorophyll concentration.	4
1.4	Mean air-sea CO ₂ flux.	5
1.5	The Southern Annular Mode.	6
2.1	Wind-, SST-, and chlorophyll-SAM relationships.	12
2.2	Ocean response to a positive SAM.	14
2.3	Regional correlations of wind, SST, and chlorophyll with the SAM.	16
3.1	Regression of 700mb geopotential height anomalies onto ENSO. .	22
3.2	Spatial patterns of variability in wind, SST, ice, and chlorophyll. .	24
3.3	PC-1 of wind, SST, ice, and chlorophyll.	28
3.4	Mean dust deposition, and regression of dust anomalies onto ENSO.	31
3.5	Biological response to SAM and ENSO.	34
4.1	Geopotential height and wind stress regressed onto the SAM. . . .	40
4.2	Regression of observed and modeled SST onto the SAM.	42
4.3	Annual-mean air-sea CO ₂ fluxes.	45
4.4	Mean Southern Ocean CO ₂ fluxes.	50
4.5	Anomalous Southern Ocean CO ₂ fluxes.	51
4.6	CO ₂ flux variance.	52
4.7	Regressions and correlations of CO ₂ fluxes with the SAM.	55
4.8	Regional regressions of CO ₂ flux and the SAM.	57
4.9	Contributions to the air-sea CO ₂ flux anomaly during positive SAM.	59
4.10	Regressions of <i>sDIC</i> and <i>pCO₂^{oc}</i> onto the SAM.	65

4.11	Mean meridional overturning, and regression on the SAM.	67
5.1	Trends in wind stress, ice fraction, and ocean $p\text{CO}_2$.	73
5.2	Trend in the SAM index.	74
5.3	Trends in the spatially-integrated Southern Ocean CO_2 fluxes.	76
5.4	Trends in CO_2 flux, and trends linearly congruent with the SAM.	77
5.5	Contributions to the trend in natural CO_2 flux.	79
5.6	Trends in surface ocean $s\text{DIC}$, $s\text{Alk}$, T , and S .	80
5.7	Trends in the anthropogenic CO_2 flux.	83
5.8	Expected and remaining anthropogenic CO_2 trends.	84

List of Tables

2.1	Regional regressions and correlations of wind, SST, and chlorophyll with the SAM.	17
3.1	Correlations of SAM and ENSO with the PC-1 of wind speed, SST, sea ice, and chlorophyll anomalies.	26
3.2	Regressions and correlations of the regional anomalies with SAM and ENSO.	29
4.1	Annual-mean air-sea CO ₂ fluxes from the model, ocean inversions, and observations.	48
4.2	Relationship between Southern Ocean CO ₂ fluxes and the SAM. .	53
4.3	Contributions to the CO ₂ flux anomaly during positive SAM.	61
4.4	Regional means and regressions with the SAM.	63
4.5	Contributions to the <i>sDIC</i> tendency.	64
5.1	Linear trends in Southern Ocean CO ₂ fluxes.	78
5.2	Estimated contributions to the total trends in natural CO ₂ flux. .	82

ACKNOWLEDGMENTS

Chapters Two and Four are versions of the following articles:

Lovenduski, N. S. and N. Gruber, 2005: Impact of the Southern Annular Mode on Southern Ocean circulation and biology. *Geophys. Res. Lett.*, **32**, L11603, doi:10.1029/2005GL022727.

Lovenduski, N. S., N. Gruber, S. C. Doney, and I. D. Lima, in press: Enhanced CO₂ outgassing in the Southern Ocean from a positive phase of the Southern Annular Mode. *Global Biogeochem. Cycles*, doi:10.1029/2006GB002900.

Copyright of both articles is with the American Geophysical Union, and permission has been granted for their reprint in this dissertation.

This research was partially supported by NASA headquarters under the Earth System Sciences Fellowship Grant NNG05GP78H.

A number of people have contributed to the development of this work. I would like to give special thanks to:

- Prof. Niki Gruber for his patient and kind guidance these past five years. One could not ask for a better advisor.
- Prof. Jim McWilliams for his helpful mentoring during Niki's absence.
- Dr. Scott Doney and Dr. Ivan Lima for access to the model output used in Chapters Four and Five, and for providing answers to my numerous modeling questions.
- The past and present members of the biogeochemistry group at UCLA for their infinite assistance.
- Brian Medeiros, for countless hours of reassurance and encouragement during graduate school.
- My parents, for their love and support throughout my entire education.

VITA

March 22, 1979 Born, Englewood, New Jersey

2001 B.A., Earth and Planetary Science
Washington University in St. Louis

2003 M.S., Atmospheric Sciences
University of California, Los Angeles

2004 C. Phil., Atmospheric Sciences
University of California, Los Angeles

PUBLICATIONS

Ehlmann, B. L., R.E. Arvidson, B. L. Jolliff, S. S. Johnson, B. Ebel, N. Lovenduski, J. D. Morris, J. A. Byers, N. O. Snider, and R. E. Criss, 2005: Hydrologic and Isotopic Modeling of Alpine Lake Waiau, Mauna Kea, Hawai'i. *Pacific Science*, **59**(1), 1-15.

Lovenduski, N. S., and N. Gruber, 2005: Impact of the Southern Annular Mode on Southern Ocean circulation and biology. *Geophysical Research Letters*, **32**, L11603, doi:10.1029/2005GL022727.

Lovenduski, N. S., N. Gruber, S. C. Doney, and I. D. Lima, in press: Enhanced CO₂ outgassing in the Southern Ocean from a positive phase of the Southern Annular Mode. *Global Biogeochemical Cycles*, doi:10.1029/2006GB002900.

ABSTRACT OF THE DISSERTATION

Impact of the Southern Annular Mode on Southern Ocean Circulation and Biogeochemistry

by

Nicole Suzanne Lovenduski

Doctor of Philosophy in Atmospheric Sciences

University of California, Los Angeles, 2007

Professor Nicolas Gruber, Co-chair

Professor James C. McWilliams, Co-chair

The Southern Annular Mode (SAM) is the leading mode of atmospheric interannual variability over the entire Southern Hemisphere, yet the impact of the SAM and its trend on Southern Ocean circulation and biogeochemistry is largely unknown. Using satellite observations and a numerical model, this dissertation investigates the role of the SAM in driving variability and trends in the circulation, biological activity, and carbon cycling in the Southern Ocean. A large fraction of the variability in the Southern Ocean circulation is found to be linked to the SAM. Positive phases of the SAM are associated with a poleward contraction of the atmospheric westerly winds, increasing the rate of upwelling, Ekman transport, and meridional overturning in the Southern Ocean. This circulation

variability causes fluctuations in surface temperature and, through modifications in light and nutrient availability, biological activity. The SAM also drives a large fraction of the variability in the flux of CO₂ between the atmosphere and Southern Ocean. The primary cause for the flux variations are anomalies in the surface concentration of dissolved inorganic carbon, due to ocean circulation changes. The long-term trend in the SAM is found to contribute to a reduction in the strength of the Southern Ocean carbon sink over the past fifty years.

Chapter 1

Introduction

The unique physical oceanography of the Southern Ocean sets the stage for its important role in the global climate system. The strong atmospheric westerly winds (Figure 1.1a) propel the flow of the Antarctic Circumpolar Current (ACC). The ACC is an eastward geostrophic current whose flow extends to great depths and spans the entire globe (Figure 1.2a), providing a pathway for the propagation of climatic signals from basin to basin and link to the global thermohaline circulation (Rintoul et al. 2001). Atmospheric westerlies also drive northward Ekman drift, creating the surface branch of an ageostrophic meridional overturning circulation known as the Deacon Cell (Figure 1.2b; Rintoul et al. 2001). Mode and intermediate water formation on the downwelling side of the Deacon Cell serves as a conduit for the transference of oceanic properties from the surface into the interior of the oceans (Banks et al. 2000), and ventilates the thermocline of the Southern Hemisphere subtropical gyres (McCartney 1982). Superimposed on these large scale Southern Ocean flows are small scale features, such as eddies and fronts. Eddies contribute to the poleward transport of heat across the ACC (Karsten and Marshall 2002), and the vertical transport of subsurface properties.

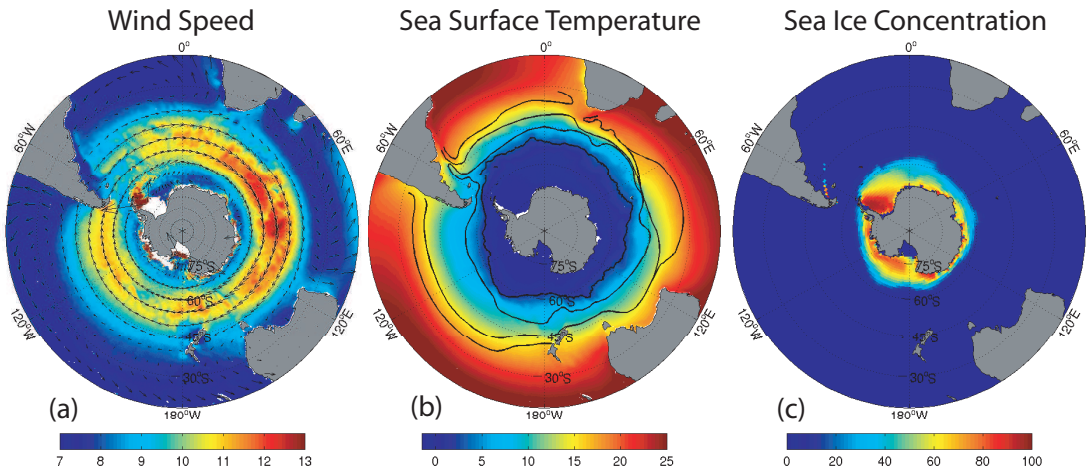


Figure 1.1: Annual-mean observed (a) wind speed (m s^{-1}) and direction from QuikSCAT (1999-2004), (b) sea surface temperature ($^{\circ}\text{C}$) from AVHRR (1985-2003), and (c) sea ice concentration (%) from SSMR & SSM/I (1979-2002). Black contours in (b) mark the location of the Southern Ocean fronts. From pole to equator these fronts are: Antarctic Polar Front (Moore et al. 1999), Subantarctic Front, South Subtropical Front, and North Subtropical Front (Belkin and Gordon 1996).

The frontal regions are defined by particularly sharp gradients in temperature (see Figure 1.1b) and salinity. Additionally, the formation of sea ice over the Antarctic continental shelf (Figure 1.1c) fuels the formation of dense bottom water, renewing the deep waters of the global oceans (Rintoul et al. 2001).

The biogeochemical cycling in the Southern Ocean is closely linked to the aforementioned circulation features. Upwelling in the Antarctic Divergence brings large amounts of macronutrients, such as nitrate (Figure 1.3a) and phosphate to the surface (Sarmiento et al. 2004), most of which remain unused due to the inefficiency of biological activity there (Boyd et al. 2000). Northward Ekman transport carries these nutrients across the ACC into the Subantarctic Zone (Sigman et al. 1999), where they become subducted in mode and intermediate water masses (Sarmiento et al. 2004). Phytoplankton production in most of the South-

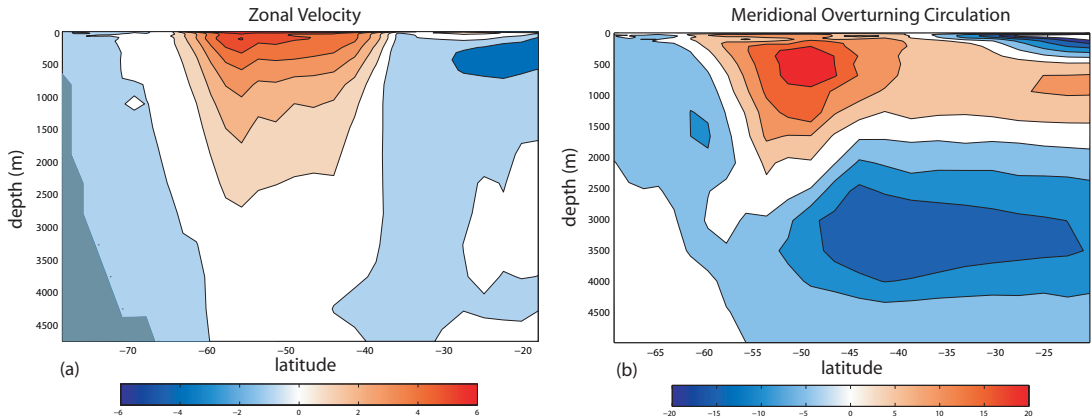


Figure 1.2: Annual-mean (a) zonal mean zonal velocity (cm s^{-1}), and (b) meridional overturning streamfunction (Sv), derived from the NCAR ocean circulation model described in Chapter 4 (1958-2004). Meridional overturning includes the Gent and McWilliams (1990) bolus parameterization velocities.

ern Ocean is thought to be limited by light and micronutrients, such as iron, rather than macronutrients (e.g. Boyd et al. 2000). As a result, phytoplankton blooms tend to occur where the circulation supplies a large amount of iron to the surface waters: near the coast, in the vicinity of the fronts, and in areas associated with seasonal ice retreat (Figure 1.3b; Moore and Abbott 2000; Sedwick and DiTullio 1997).

The rate of meridional overturning is critical to the processes regulating the exchange of CO_2 between the atmosphere and the Southern Ocean. Upwelling in the Antarctic Divergence exposes deep waters with elevated concentrations of dissolved inorganic carbon to the surface, leading to the ventilation of natural CO_2 to the atmosphere (Figure 1.4; Toggweiler and Samuels 1993; Murnane et al. 1999; Mikaloff-Fletcher et al. 2007). It has been suggested that this natural CO_2 ventilation is important for determining CO_2 on paleoclimatic timescales (Sarmiento and Toggweiler 1984; Siegenthaler and Wenk 1984). Additionally,

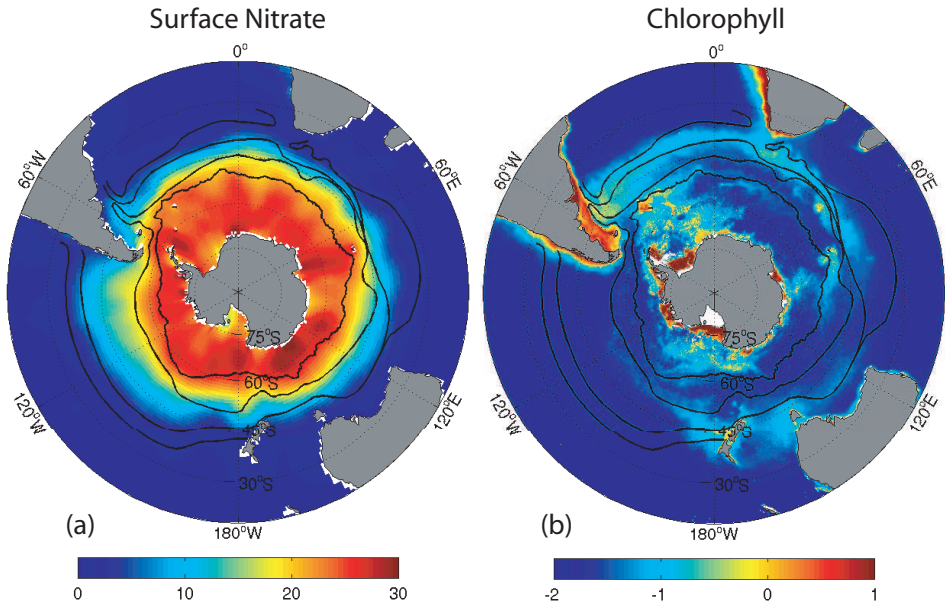


Figure 1.3: Annual-mean observed (a) surface nitrate concentration (mmol m^{-3}) from the World Ocean Atlas (Conkright et al. 2002), and (b) chlorophyll concentration ($\ln(\text{mg m}^{-3})$) from SeaWiFS (1997-2003).

approximately 40% of the global oceanic sequestration of anthropogenic CO_2 occurs on the downwelling side of the Deacon Cell (Figure 1.4), in association with the formation of mode and intermediate waters (Sabine et al. 2004; Mikaloff-Fletcher et al. 2006).

Due to its unique position, physics, and circulation characteristics, the Southern Ocean plays a critical role in the global transport of climatically significant quantities, such as heat and freshwater (Gordon 2001; Karsten and Marshall 2002), nutrients (Sarmiento et al. 2004), and carbon dioxide (CO_2) (Toggweiler and Samuels 1993; Murnane et al. 1999; Sabine et al. 2004; Mikaloff-Fletcher et al. 2006, 2007). Given the function that the Southern Ocean serves for the global climate system, and the potential for sensitivity of this region to future climate change (Sarmiento et al. 1998; Broecker et al. 1999), it is pertinent to

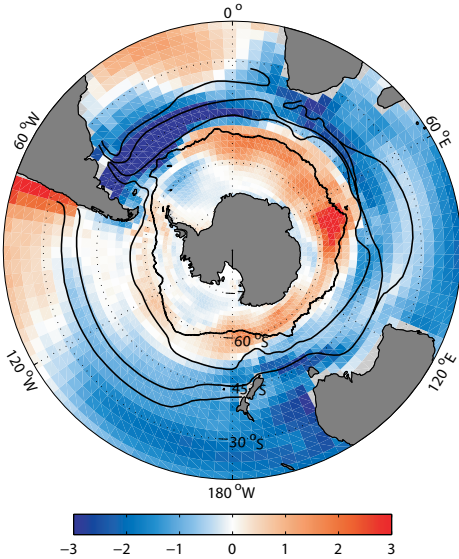


Figure 1.4: Annual-mean air-sea flux of contemporary CO₂ (mol m⁻² yr⁻¹), derived from the historic simulation of the ocean circulation and biogeochemical model described in Chapter 4 (1958-2004). Positive fluxes represent ocean outgassing, while negative fluxes represent ocean uptake of CO₂.

understand how this region responds to climate variability and how it might be affected by climate change.

Both observations (Hughes et al. 2003; Liu et al. 2004) and general circulation models (Hall and Visbeck 2002; Oke and England 2004; Watterson 2000) have shown that most of the interannual climatic variability in the Southern Ocean is closely tied to the Southern Annular Mode (SAM), the dominant mode of atmospheric interannual variability in the extratropical circulation of the Southern Hemisphere (Thompson and Wallace 2000). The spatial pattern associated with the SAM represents a nearly zonally symmetric oscillation of pressure over the Pole and pressure over midlatitudes (Figure 1.5a). The SAM index is defined as the leading principal component of atmospheric geopotential height anomalies south of 20°S, such that positive SAM is associated with anomalously low

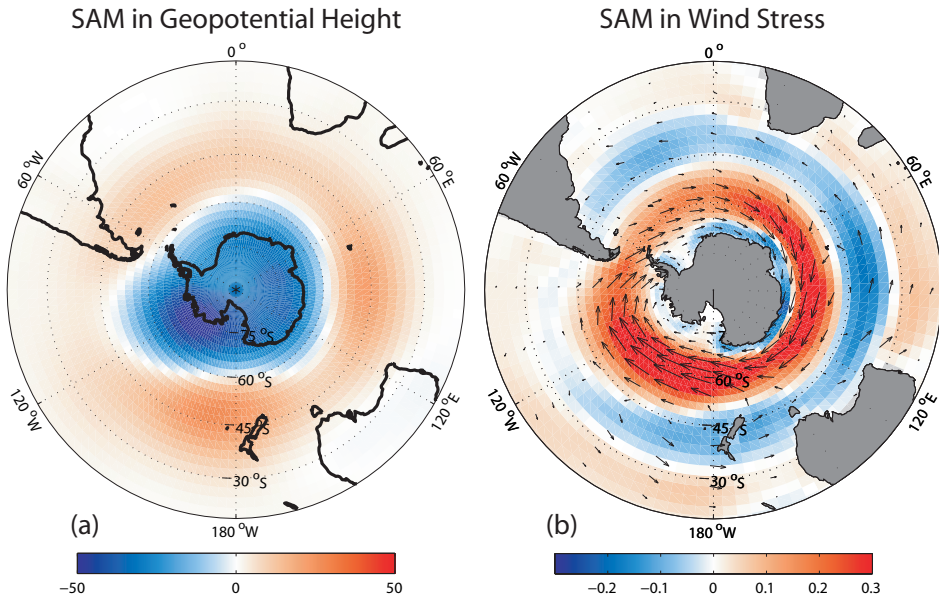


Figure 1.5: Regressions of (a) 700mb geopotential height anomalies (m), and (b) wind stress anomalies (dyne cm^{-2}) onto the SAM index, derived from the NCEP/NCAR reanalysis (1958-2004; Kalnay et al. 1996).

pressure over the Pole. Such a positive SAM is also coincident with a poleward shift of the westerly winds (Figure 1.5b; Hartmann and Lo 1998; Limpasuvan and Hartmann 1999). Over the past 30 years, the SAM has exhibited a positive trend, corresponding to a poleward strengthening of the winds with time (Thompson et al. 2000; Thompson and Solomon 2002). As the atmospheric westerly winds are responsible for driving the circulation of the Southern Ocean, the SAM has the capacity to cause variability and trends in the oceanic circulation.

This dissertation is focused on understanding variability and trends in Southern Ocean circulation and biogeochemical cycling, with particular emphasis on the role of the SAM. Changes in the Southern Ocean circulation in association with the SAM have the potential to influence nutrient supply, phytoplankton abundance, and carbon cycling, yet the impact of the SAM on Southern Ocean

biogeochemistry is not well understood. In-situ measurements of the Southern Ocean remain somewhat scarce. To overcome this limitation, satellite products and numerical models are used here to investigate coherent variability and trends over large spatial and temporal scales.

Chapter 2 takes advantage of satellite-derived wind speed and direction, sea surface temperature, and chlorophyll-*a* concentration to examine the relationship between the SAM and Southern Ocean circulation and phytoplankton abundance on intraseasonal to interannual timescales. These same satellite observations are utilized in Chapter 3 to find large scale patterns of variability in the Southern Ocean and investigate their link to the SAM and another mode of atmospheric variability, the El Niño-Southern Oscillation. In Chapters 4 and 5, output from an ocean physical-biogeochemical-ecological model is used to research the impact of variability and trends in the SAM on the flux of CO₂ between the atmosphere and the Southern Ocean. The dissertation is concluded in Chapter 6, where results from the previous chapters are placed into a global context and the discussion of the results is extended to global climate change.

Chapter 2

Impact of the Southern Annular Mode on Southern Ocean circulation and biology

2.1 Abstract

We investigate the impact of the Southern Annular Mode (SAM) on surface wind, sea surface temperature (SST), and surface chlorophyll concentration on intraseasonal to interannual timescales in the Southern Ocean using 8-day average satellite observations. Positive phases of the SAM are associated with enhanced westerly winds over the Antarctic Zone (AZ) and Polar Frontal Zone, driving increased equatorward Ekman transport and cold SST anomalies in these regions. Positive SAM is also associated with easterly wind and warm SST anomalies in the Subtropical Zone. South of the Antarctic Polar Front (APF), chlorophyll concentration anomalies are positively correlated with the SAM, however this correlation is negative north of the APF. We suggest that the positive correlation in the AZ is due to the increased supply of iron by upwelling, while the negative correlation north of the APF is caused by stronger light limitation as a

consequence of deeper mixed layers.

2.2 Introduction

The SAM, or the Antarctic Oscillation, is the leading mode of climate variability on timescales from intraseasonal to interannual over the entire Southern Hemisphere (Thompson and Wallace 2000). It is characterized by a large-scale alternation of atmospheric mass between the mid- and high-latitudes, and is associated with a meridional shift in the atmospheric westerly winds (Hartmann and Lo 1998). These westerly winds are responsible for driving the circulation of the Southern Ocean, and it has been shown using general circulation models that wind shifts associated with the SAM alter Southern Ocean circulation patterns substantially (Hall and Visbeck 2002; Oke and England 2004; Watterson 2000). Changes in circulation can affect phytoplankton abundance and biogeochemical cycling in this region, yet the impact of the SAM on them has not yet been documented.

The Southern Ocean plays a critical role in the global climate system. The strong wind-driven eastward flow of the Antarctic Circumpolar Current connects the Pacific, Atlantic, and Indian ocean basins. In addition, the Southern Ocean meridional overturning circulation contributes substantially to the global transport of climatically significant quantities such as heat, fresh water, nutrients, and anthropogenic CO₂ (Rintoul et al. 2001; Sarmiento et al. 2004). Mode waters transfer these quantities from the surface into the interior of the oceans (Banks et al. 2000) and ventilate the thermocline of the Southern Hemisphere subtropical gyres (McCartney 1982). Nearly 40% of global anthropogenic CO₂ uptake

is associated with this pathway (Sabine et al. 2004), substantially offsetting the outgassing of natural CO₂ (Gloor et al. 2003). However, very little is known about how this region varies in response to climate variability and how it may be affected by climate change.

Given the paucity of in situ data in the Southern Ocean, satellite products provide us with one of the few means to investigate coherent variability over large spatial and temporal scales. This study takes advantage of satellite-derived wind speed and direction, SST, and chlorophyll-*a* concentration to examine the relationship between the SAM and Southern Ocean circulation and phytoplankton abundance on intraseasonal to interannual timescales.

2.3 Data sources and analysis

We used satellite observations of: (1) daily wind speed and direction from QuikSCAT on a 25 km grid from 1999-2004, (2) 8-day averaged equal angle best SST from AVHRR Oceans Pathfinder (versions 4.1 and interim 4.1) on a 9 km grid from 1985-2003, and (3) 8-day averaged chlorophyll-*a* concentration from SeaWiFS on a 9 km grid from 1997-2004. Since oceanic chlorophyll concentration is approximately lognormally distributed (Campbell 1995), the natural log transformation was applied to the SeaWiFS data and means were computed from the transformed data. The surface wind was averaged into 8-day periods, and all 3 data sets were interpolated to a 1° grid using a linear interpolation scheme. The data were deseasonalized by removing the climatological mean seasonal cycle computed by binning all data into 46 8-day bins and then taking the average. A linear trend was removed at each grid cell in order to remove any non-stationarity. Missing

data were ignored in all calculations. The daily Antarctic Oscillation index from 1979-2004 was also averaged into 8-day periods, standardized by the standard deviation, and linearly detrended as above.

We investigate the impact of the SAM on circulation and biology using regression and correlation analysis. To maximize the statistical significance given the short and differing length of the records, we performed this analysis over the period of time for which the data sets overlap. We assume that the correlation is stationary, i.e. it is not changing with time. The statistical significance of all correlation coefficients was determined considering the autocorrelation present in our 8-day anomalies. This is accounted for by replacing the t statistic sample size, N , with an effective sample size, N_{eff} :

$$N_{\text{eff}} = N \left(\frac{1 - r_1 r_2}{1 + r_1 r_2} \right) \quad (2.1)$$

where r_1 and r_2 are the lag-1 autocorrelation coefficients of the time series being correlated (Bretherton et al. 1999).

2.4 Results and discussion

The SAM index is defined by the leading principal component of the 700 mb geopotential height south of 20°S in the atmosphere. Positive SAM is associated with negative pressure anomalies over Antarctica, positive pressure anomalies over the mid-latitudes, and a strengthening of the zonal atmospheric pressure gradient. We find that the anomalously strong pressure gradient during positive SAM acts to significantly strengthen the westerly winds at $\sim 55^{\circ}\text{S}$, and to weaken

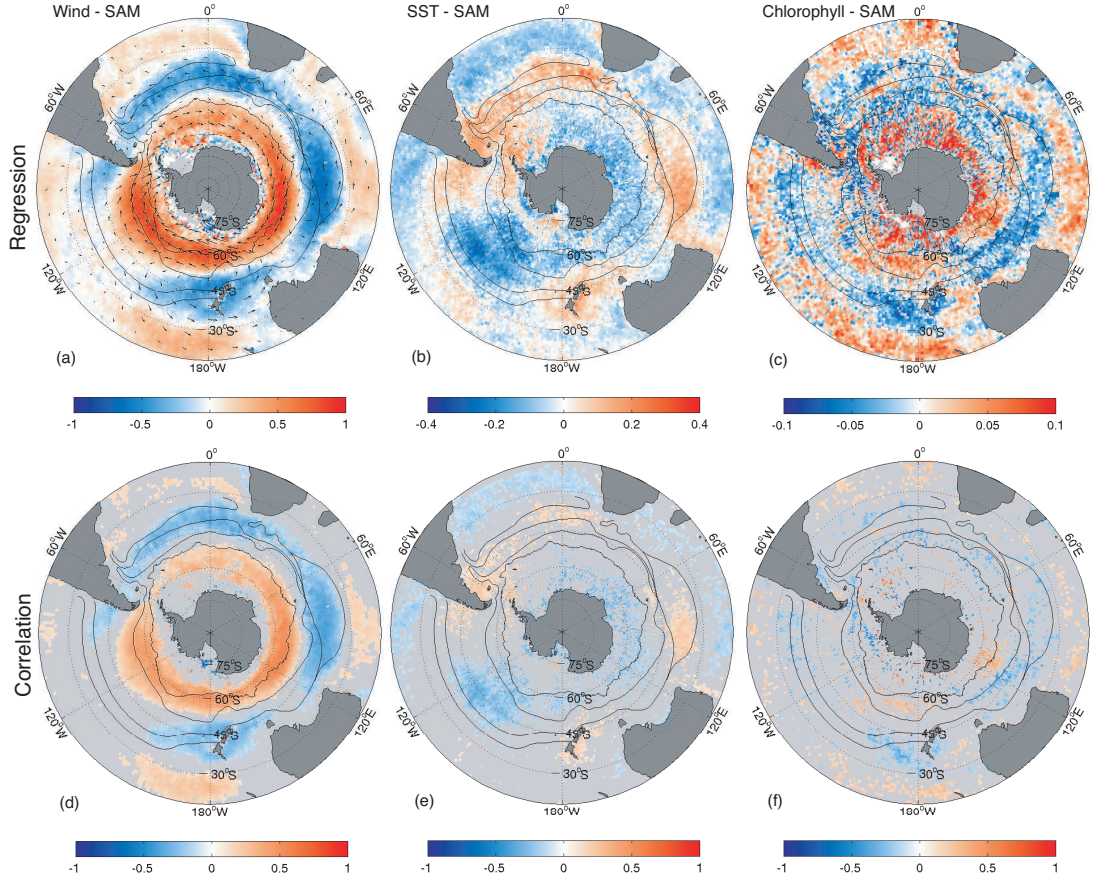


Figure 2.1: Maps of (a)-(c) regressions and (d)-(f) correlations between the SAM index and (a)&(d) wind speed and (a) direction; (b)&(e) SST; and (c)&(f) chlorophyll concentration. The regression coefficients indicate changes in the wind speed (m s^{-1}), SST ($^{\circ}\text{C}$), and natural log of the chlorophyll concentration [$\ln(\text{mg m}^{-3})$] corresponding to one standard deviation change in the SAM index. Only those correlation coefficients with significance $\geq 95\%$ are shown. Black contours mark the location of the Southern Ocean fronts. From pole to equator these fronts are: Antarctic Polar Front (Moore et al. 1999), Subantarctic Front, South Subtropical Front, and North Subtropical Front (Belkin and Gordon 1996).

the westerly winds (easterly anomaly) at $\sim 35^{\circ}\text{S}$, by as much as 0.9 m s^{-1} in some regions (Figure 2.1a,d), confirming previous results (see Hartmann and Lo (1998), Limpasuvan and Hartmann (1999)). This poleward contraction of the westerlies during positive SAM persists throughout all seasons, but is strongest during austral summer.

Figure 2.2 illustrates how the oceanic circulation is expected to change in response to the strengthening and shifting of the wind during positive SAM (see Hall and Visbeck 2002). Surface westerly wind anomalies generate northward Ekman transport anomalies in the Antarctic Zone (AZ), the region south of the Antarctic Polar Front (APF; $\sim 55^{\circ}\text{S}$), and Polar Frontal Zone (PFZ), the region between the APF and the Subantarctic Front (SAF), enhancing the divergence and driving increased upwelling of water from below. Surface easterly wind anomalies produce southward Ekman transport anomalies in the Subtropical Zone (STZ), the region between the North and South Subtropical Fronts (NSTF & SSTF). The increased convergence of water in the Subantarctic Zone (SAZ), the region between the SAF and SSTF, increases downwelling of water from the surface to depth. We therefore expect the anomalous Ekman transport to generate negative SST anomalies in the AZ and PFZ, and positive SST anomalies in the STZ (Figure 2.2).

Our satellite-based analysis confirms these expectations by showing that a positive SAM is associated with a significant decrease in SST in the AZ and PFZ, and a significant increase in SST in the STZ (Figure 2.1b,e; Figure 2.3; Table 2.1). As is the case for the westerly wind, this SST response is most pronounced during austral summer. The SST response pattern is nearly zonally

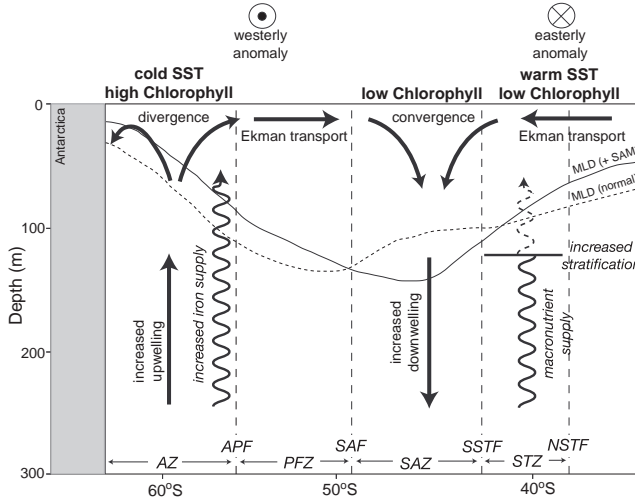


Figure 2.2: Schematic illustration of the upper ocean response to a positive phase of the SAM.

symmetric, the exception being the Pacific sector ($\sim 100^{\circ}\text{W} - 160^{\circ}\text{W}$), where a positive SAM is associated with negative SST anomalies across all 4 Southern Ocean zones (Figure 2.1b). This response may be associated with other climate variations that overwhelm the impact of SAM but have some correlation with Southern Ocean circulation, e.g. ENSO (Garreaud and Battisti 1999) and its connection to the Antarctic Dipole Pattern (Liu et al. 2002), and the Antarctic Circumpolar Wave (White and Peterson 1996).

In the AZ, SAM and chlorophyll are positively correlated, and regression coefficients often exceed 0.1 mg m^{-3} per standard deviation (Figure 2.1c). Conversely, the remaining 3 Southern Ocean zones tend to experience a decrease in chlorophyll concentration during positive phases of the SAM (Figure 2.1; Table 2.1). While this negative response dominates north of the APF, it is not entirely zonally symmetric. The strongest response is found in the SAZ south of Australia where regression coefficients can be as large as -0.06 mg m^{-3} per standard deviation,

corresponding to 34% of the mean chlorophyll value in this region. Elsewhere, correlations are relatively low and often not statistically significant (Figure 2.1f). We attribute this low level of significance primarily to the shortness of the record and the non-uniform chlorophyll coverage due to high incidence of cloud cover (e.g. $\overline{N_{\text{eff},\text{AZ}}} \approx 30$; $\overline{N_{\text{eff},\text{SAZ}}} \approx 90$).

In order to better understand the biological response to circulation changes associated with the SAM, we investigate the relationship between chlorophyll concentration and SST anomalies in the Southern Ocean. At latitudes typically associated with the AZ, anomalies of chlorophyll concentration and SST are negatively correlated (Figure 2.3), suggesting that when cold, nutrient-rich water upwells, phytoplankton abundance tends to increase. Since biological productivity in this region of the Southern Ocean is thought to be limited by micronutrients (Boyd et al. 2000), this negative chlorophyll-SST correlation may be related to iron supply from below. There is little correlation between anomalies of chlorophyll and SST in the SAZ (Figure 2.3). Since this region is characterized by deep mixed layers (Kara et al. 2003), this lack of correlation could indicate that biological productivity in this region is limited by light. In the subtropical waters within and equatorward of the STZ, biological production is limited by macronutrients (Figure 2.3) and stratification is dominated by temperature (Pollard et al. 2002).

The biological response to the SAM can be explained by considering the consequences of the circulation changes (Figure 2.2). We propose that during positive SAM the increase in phytoplankton abundance in the AZ is driven by the anomalous upwelling of iron, while the decrease in chlorophyll concentration in the SAZ

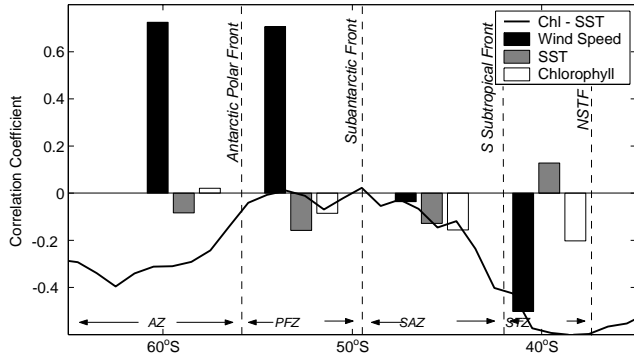


Figure 2.3: The correlation coefficient of the SAM index with the average time series of wind speed, SST, and chlorophyll concentration anomalies. The anomaly time series were averaged over various regions in the Southern Ocean, defined by the Southern Ocean fronts. Overlain is the correlation coefficient of the zonal-mean SST and chlorophyll concentration anomalies.

is caused by deeper mixed layers and increased light limitation. We note that nonlinear effects such as photoadaptation could be confounding correlations in the SAZ. The decrease in chlorophyll concentration in the STZ during positive SAM can be explained by warmer than normal SST (Figure 2.1b; Figure 2.3) and increased stratification, leading to reduced macronutrient supply in this region.

On the basis of a suite of remotely sensed products, we suggest the following sequence of events in response to a positive phase of the SAM (Figure 2.2): The poleward shift of the surface westerly winds creates anomalies in both poleward and equatorward Ekman transport, driving increased upwelling of cold, iron-enriched water into the AZ, and increasing convergence and downwelling in the SAZ. The former process slightly increases the phytoplankton abundance in the AZ, while the latter processes deepens the mixed layer and decreases the chlorophyll concentration in the SAZ. In the STZ, increased stratification from warm SST anomalies reduces macronutrient supply and decreases chlorophyll

Table 2.1: Mean values and regression and correlation coefficients of the mean anomaly time series with the SAM index. Regression coefficients correspond to one standard deviation change in the SAM index.

Zone	Mean value	Regression coefficient associated with $1\sigma_{SAM}$	Correlation with SAM index
<i>Wind Speed [m s⁻¹]</i>			
AZ	10.0	0.45	0.73
PFZ	10.8	0.39	0.71
SAZ	10.1	-0.02	-0.04
STZ	8.9	-0.03	-0.50
<i>SST [°C]</i>			
AZ	-0.4	-0.024	-0.08
PFZ	4.3	-0.041	-0.16
SAZ	9.6	-0.028	-0.13
STZ	14.8	0.032	0.13
<i>Chlorophyll [mg m⁻³]</i>			
AZ	0.2029	0.0020	0.02
PFZ	0.1876	-0.0061	-0.09
SAZ	0.1748	-0.0075	-0.16
STZ	0.1770	-0.0120	-0.20

concentration.

2.5 Impact on carbon cycle

Can we use these relationships to deduce something about the impact of the SAM on the air-sea CO₂ flux in the Southern Ocean? During positive phases of the SAM, we suspect that the anomalous upwelling of waters rich in dissolved inorganic carbon in the AZ is elevating the partial pressure of CO₂ in the surface waters. The resulting anomalous outgassing may, however, be mitigated by increased CO₂ solubility and biological productivity in this region. Positive SAM increases convergence and downwelling in the mode water formation regions of the Southern Ocean, possibly accelerating the pathway for the subduction and

equatorward transport of anthropogenic CO₂. However, the anomalous uptake of CO₂ may be offset by decreased biological production in this region. Overall, we therefore expect only a moderate level of air-sea CO₂ flux variability.

2.6 Conclusions

Despite the relatively short length and sometimes sparseness of the observation record, we have demonstrated that statistically significant relationships between the satellite observations and the SAM exist. These relationships can be interpreted with a conceptual model (Figure 2.2), which suggests a substantial response of ocean circulation and biology to variations in the SAM.

Several studies have drawn our attention to the trend toward positive SAM over the past 30 years, which may be linked to climate change and ozone depletion in high latitudes (Thompson et al. 2000; Thompson and Solomon 2002). The impact of this trend on ocean circulation and the global carbon cycle is poorly understood, but may be indicative of how this system might respond to future climate change.

Chapter 3

Large scale patterns of variability in the Southern Ocean

3.1 Abstract

We investigate the large scale patterns of variability in Southern Ocean wind speed, sea surface temperature (SST), sea ice concentration, and chlorophyll concentration on the basis of 8-day averaged satellite observations. The dominant modes of variability in each variable, determined by empirical orthogonal function analysis, are closely linked to the Southern Annular Mode (SAM) and the El Niño-Southern Oscillation (ENSO). Significant correlations between ENSO and wind speed, SST, and sea ice exist in the Southern Ocean, confirming previous findings. As with the SAM, we find that ENSO also has a significant impact on Southern Ocean chlorophyll concentrations, likely due to ocean circulation changes that alter light and nutrient supplies. These mechanisms are similar to the ones driving chlorophyll variability in association with the SAM. We conclude that SAM and ENSO are both important drivers of large scale variability in the Southern Ocean. For wind speed, SAM is more important, for SST, ENSO tends

to dominate, whereas for chlorophyll, SAM and ENSO explain a similar amount of the observed variance.

3.2 Introduction

Interannual variability in the Southern Hemisphere atmosphere is primarily controlled by two phenomena: the Southern Annular Mode (SAM) and remote connections to the El Niño-Southern Oscillation (ENSO) pattern (Kidson 1999). The SAM is the dominant mode of climate variability in the Southern Hemisphere, explaining nearly 30% of atmospheric pressure variations south of 20°S (Thompson and Wallace 2000). ENSO has been shown to contribute to a large fraction of atmospheric variability in the Southern Hemisphere as well (Turner 2004). The previous chapter of this dissertation focused on understanding the nature of the relationships between the SAM and Southern Ocean circulation and biology. While the SAM was found to have strong relationships with wind speed, sea surface temperature (SST), and chlorophyll concentration, it captured less than half of the variability in SST and chlorophyll, suggesting that other atmospheric phenomena such as ENSO could be responsible for creating anomalies in these fields.

ENSO is primarily a tropical Pacific phenomenon, characterized by atmospheric pressure and surface temperature oscillations across the basin. Warm ENSO (El Niño) events are associated with a weakening of the easterly trade winds and a subsequent eastward propagation of warm SST anomalies, which drives enhanced convection in the central tropical Pacific (McPhaden et al. 2006). While ENSO variability occurs in the tropical Pacific, it has teleconnections to

other regions of the world (Trenberth et al. 1998), and therefore could be linked to variability in the Southern Ocean. The enhanced convection in the Pacific during warm ENSO events and the associated meridional advection of anomalies in potential vorticity can excite a pattern of Rossby waves which force an anomalous anticyclonic circulation near 60°S in the eastern Pacific (see, e.g. Figure 3.1; Mo and Higgins 1998; Garreaud and Battisti 1999; Kidson and Renwick 2002; Carleton 2003; Simmonds and King 2004; Turner 2004; Fogt and Bromwich 2006). This teleconnection pattern is also known as the Pacific-South American (PSA) pattern (Mo and Ghil 1987). The PSA has a large influence on the atmospheric circulation in the Pacific sector of the Southern Ocean, and has been connected with air temperature variability on the Antarctic Peninsula (Kwok and Comiso 2002). In addition to the PSA teleconnection in the Pacific, recent evidence suggests that during the austral summer, ENSO can induce changes in the winds over the Southern Ocean at all longitudes (Robinson 2002; Seager et al. 2003; L'Heureux and Thompson 2006). This zonally symmetric response is thought to be a consequence of ENSO-related variations in the strength of the subtropical zonal flow, which alters the equatorward eddy propagation in the upper troposphere. This creates anomalies in the latitude of maximum eddy dissipation, ultimately driving a meridional shift in the westerlies (Robinson 2002; Seager et al. 2003; L'Heureux and Thompson 2006).

In addition to the mentioned changes in wind speed, ENSO has also previously been linked to SST and sea ice variability in the Southern Ocean (Garreaud and Battisti 1999; Yuan and Martinson 2000). SST anomalies associated with ENSO have been shown to be caused by anomalous sensible and latent heat ex-

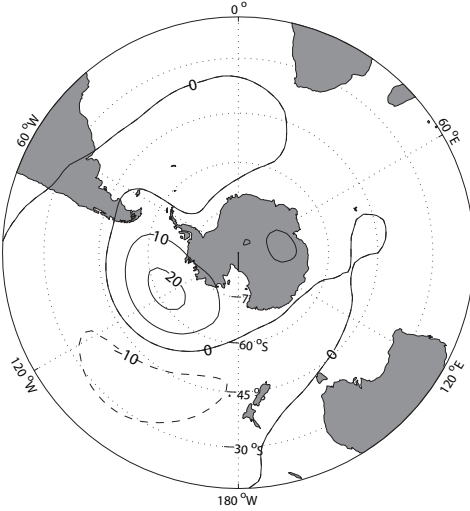


Figure 3.1: Regression of 700mb atmospheric geopotential height anomalies onto the ENSO index (m).

change with the atmosphere and by anomalies in ocean circulation (Ciasto and Thompson, in press; Verdy et al. 2006; Garreaud and Battisti 1999). ENSO-related variations in air temperature are also thought to drive sea ice concentration anomalies in the eastern Pacific and near the Antarctic Peninsula (Yuan and Martinson 2000; Liu et al. 2002; Kwok and Comiso 2002; Lefebvre et al. 2004; Liu et al. 2004; Yuan 2004). Since oceanic biological activity, and hence chlorophyll concentration, is sensitive to parameters such as wind speed, SST, and sea ice concentration, it seems likely that ENSO variability could also impact chlorophyll in the Southern Ocean. In conjunction with the variability associated with the SAM, there is the potential for these two phenomena to explain a large fraction of the overall variance in the Southern Ocean.

In this chapter, we examine the large scale patterns of variability in Southern Ocean wind speed, SST, sea ice concentration, and chlorophyll concentration. As both SAM and ENSO are thought to drive anomalies in these fields, we investigate

how the dominant modes of variability are linked to the two phenomena. We review the impact of ENSO on wind speed, SST, and sea ice concentration, and elucidate the mechanisms by which ENSO can impact chlorophyll concentration in the Southern Ocean.

3.3 Methods

The wind speed, SST, and chlorophyll concentration data used for this study are identical to those used in the previous chapter of this dissertation. All are 8-day averaged, 1° interpolated fields. As in the previous chapter, anomalies in these fields are calculated by removing the seasonal cycle and linear trend from the data at each grid cell. In this analysis, we also use sea ice concentration data from SMMR and SSM/I (Cavalieri et al. 2002). Daily ice concentrations are averaged into 8-day periods, and trends and seasonal cycles are removed as above to create anomalies. Analysis is conducted over the periods of time for which data are available: wind speed from 1999 to 2004, SST from 1985 to 2003, sea ice from 1979 to 2002, and chlorophyll from 1997 to 2004.

We ascertain the dominant modes of variability in each data set by performing empirical orthogonal function (EOF) analysis, as described in Wilks (1995). EOF analysis is done on spatial subsets of the data: for wind speed, SST, and chlorophyll, the region is limited to the southern hemisphere south of 20°S ; for sea ice, only the region south of 60°S is considered. Anomalies in each data set are weighted by $\sqrt{\cos \phi}$, where ϕ is latitude in radians, and put into anomaly matrices with dimensions of time by space. The spatial covariance of each cosine-weighted data set is found by multiplying the anomaly matrix by its transpose. Eigenanal-

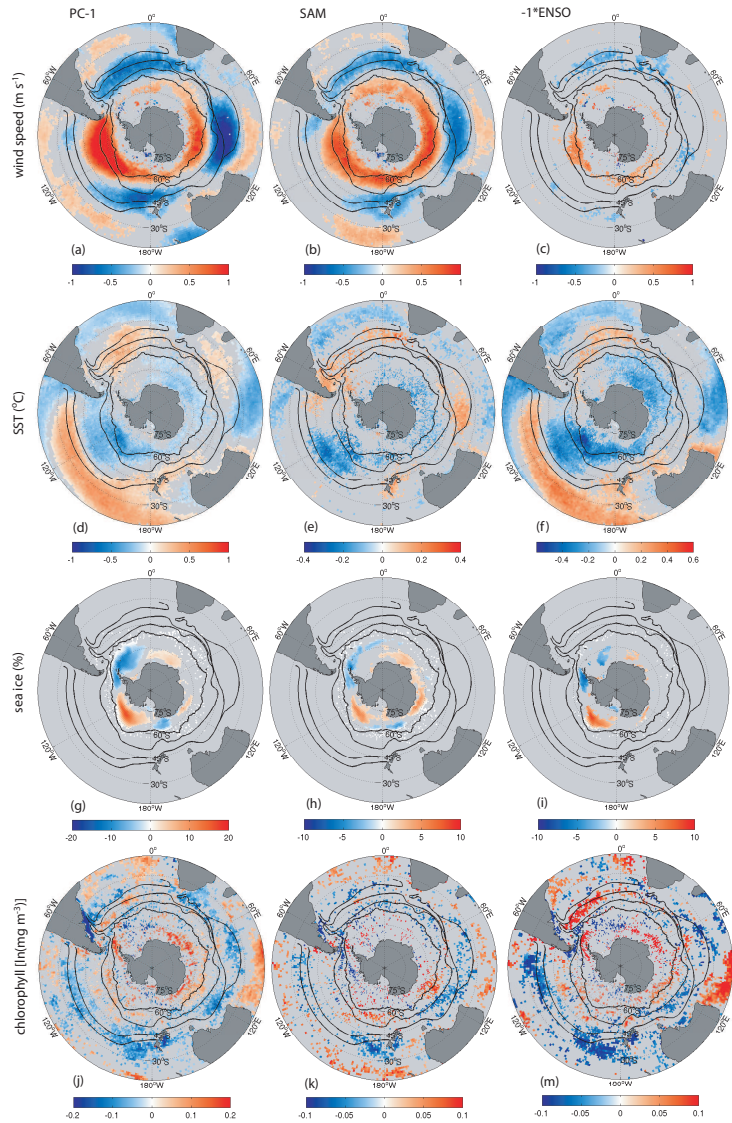


Figure 3.2: Regressions of (1^{st} row) wind speed, (2^{nd} row) SST, (3^{rd} row) sea ice concentration, and (4^{th} row) chlorophyll concentration anomalies onto (1st column) the first principal component of that variable, (2nd column) the SAM index, and (3rd column) the inverted ENSO index. Regression coefficients indicate changes in wind speed (m s^{-1}), SST ($^{\circ}\text{C}$), sea ice concentration (%), and natural log of the chlorophyll concentration [$\ln(\text{mg m}^{-3})$] corresponding to one standard deviation change in the time series. Only those regressions whose correlations exceed 95% statistical significance are plotted. SST and chlorophyll PCs cannot be considered separable from their second PCs. Black contours mark the location of the Southern Ocean fronts, as in the previous chapter.

ysis is conducted on the covariance matrix in order to determine the eigenvectors (principal components, PCs) and their associated eigenvalues. We depict spatial patterns associated with each eigenvector as regression maps of anomalies in each data set onto their associated, standardized PCs. We use the North et al. (1982) criterion to determine the 95% confidence error in the estimation of the eigenvalues. If the eigenvalues of adjacent EOFs are within these confidence bounds, the associated PCs are not considered separable or significant.

The SAM index used in this analysis is the 8-day averaged index from the NOAA Climate Prediction Center, and is identical to that used in the previous chapter. An 8-day ENSO index was constructed by averaging observed 8-day SST anomalies over the Niño3.4 region (5°N - 5°S , 120°W - 170°W). Positive phases of the ENSO index correspond to warm (El Niño) events. Both indices are standardized by subtraction of their mean and division by their standard deviation.

3.4 Modes of variability

The patterns associated with the leading modes of variability in wind speed, SST, sea-ice concentration and chlorophyll concentration south of 20°S are shown in the first column of Figure 3.2. While the dominant modes do not capture a large percentage of the variability in each field (8%, 7%, 10%, and 4% in wind speed, SST, sea ice, and chlorophyll, respectively), their spatial patterns are rather reminiscent of the SAM regressions from the previous chapter. Indeed, the second column of Figure 3.2 indicates that these dominant modes of variability are connected to the SAM. The strongest link between the two patterns is in the wind speed field, where the SAM explains nearly 45% (r^2) of the variance in PC-1

Table 3.1: The correlation coefficient of the SAM and ENSO with the first principal component (PC-1) of 8-day averaged wind speed, SST, sea ice concentration, and chlorophyll concentration anomalies. Statistical significance is indicated by boldface type.

Variable	$r_{PC-1,SAM}$	$r_{PC-1,ENSO}$
Wind Speed	0.65	-0.24
SST	0.13	-0.68
Sea Ice	0.30	-0.40
Chlorophyll	0.30	-0.51

(Table 3.1). The SAM also has a significant correlation with the first PC of SST, sea ice, and chlorophyll, but the variance in PC-1 that can be attributed to the SAM is actually quite low in these fields (Table 3.1).

As shown in the third column of Figure 3.2, the regressions of all four variables with ENSO also tend to agree with the spatial patterns associated with PC-1. This is particularly true for SST, sea ice, and chlorophyll, where ENSO explains ~45%, 15%, and 25% of the variance in PC-1, respectively (Table 3.1). In fact, more of the variance in the first PC of SST, sea ice, and chlorophyll can be explained by ENSO than SAM (Table 3.1). A closer investigation of the PC-1 time series of each variable (Figure 3.3) demonstrates that while PC-1 of wind speed exhibits high-frequency variability (as does the SAM index), PC-1 of SST, ice, and chlorophyll exhibit variability over lower frequencies. In fact, the spectra of the latter three time series (not shown) peaks in the 3-7 year band, as does the spectra of ENSO.

3.5 Causes of the variability

In Chapter 2, we investigated the connection between the SAM and Southern Ocean wind speed, SST, and chlorophyll concentration. We used a conceptual model (see Figure 2.2) to explain the impact of the SAM on these variables. However, the results from Section 3.4 suggest that ENSO could also play an important role in controlling variability. Here we focus on understanding the impact of ENSO on these variables. We will compare and contrast the response of the Southern Ocean to both SAM and ENSO in the next section.

We further examine the nature of the relationship between ENSO and wind speed, SST, sea ice, and chlorophyll with regression analysis (third column of Figure 3.2 (note that regressions here are on the negative ENSO index) and the last two columns of Table 3.2). Warm phases of ENSO are associated with negative wind speed anomalies in the PFZ, and increased wind speed in the STZ. A weak zonal symmetry is evident in the wind-ENSO regression patterns (Figure 3.2c), providing evidence for the atmospheric mechanisms described by Robinson (2002), Seager et al. (2003), and L'Heureux and Thompson (2006), whereby cold ENSO events are accompanied by an increase (decrease) in westerly wind stress at 55°S (35°S).

ENSO is strongly correlated with SST throughout much of the Southern Ocean (Figure 3.2f), supporting the previous findings in the literature (Ciasto and Thompson, in press; Verdy et al. 2006; Garreaud and Battisti 1999). In the AZ, cold ENSO events are associated with colder than normal SSTs with near-zonal uniformity. SST anomalies are also strongly correlated with ENSO in the

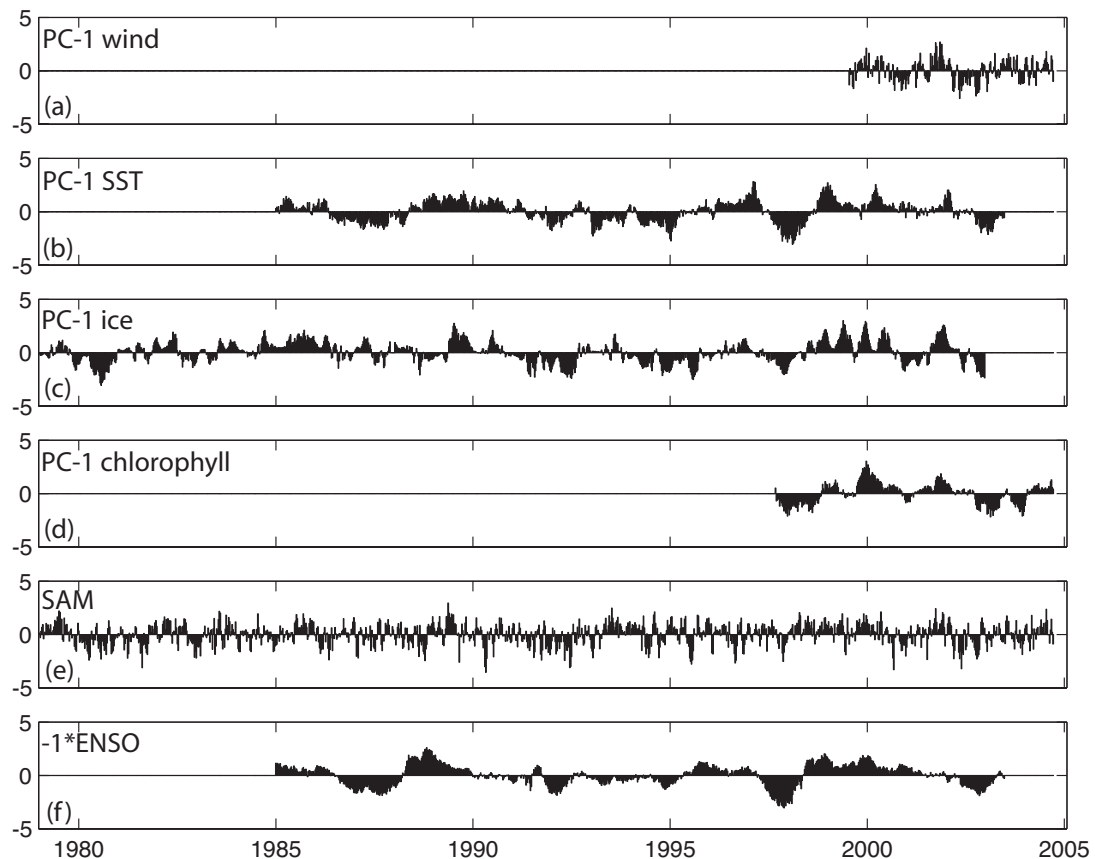


Figure 3.3: Time series of the standardized first principal component of (a) wind speed, (b) SST, (c) sea ice concentration, and (d) chlorophyll concentration anomalies south of 20°S (60°S for ice), and standardized (e) SAM and (f) inverted ENSO indices.

Table 3.2: Regression and correlation coefficients of the mean anomaly time series with SAM and ENSO. Statistically significant coefficients indicated in boldface.

Zone	SAM		ENSO	
	Regression	Correlation	Regression	Correlation
<i>Wind Speed [m s⁻¹]</i>				
AZ	0.45	0.73	-0.15	-0.21
PFZ	0.39	0.71	-0.15	-0.23
SAZ	-0.02	-0.04	0.03	0.06
STZ	-0.03	-0.50	0.15	0.22
<i>SST [°C]</i>				
AZ	-0.02	-0.08	0.11	0.38
PFZ	-0.04	-0.16	0.10	0.38
SAZ	-0.03	-0.13	0.05	0.25
STZ	0.03	0.13	-0.02	-0.06
<i>Chlorophyll [mg m⁻³]</i>				
AZ	0.0020	0.02	-0.0123	-0.15
PFZ	-0.0061	-0.09	0.0050	0.09
SAZ	-0.0075	-0.16	0.0009	0.02
STZ	-0.0120	-0.20	0.0113	0.22

PFZ and SAZ, although this relationship is strongest in the Pacific sector. In the subtropical Pacific, cold ENSO events are linked to warm SST. Both Verdy et al. (2006) and Ciasto and Thompson (in press) attribute the Southern Ocean SST-ENSO regression patterns to changes in the sensible and latent heat fluxes and anomalies in Ekman transport. Anomalous advection of heat and moisture in the atmosphere via the PSA teleconnection pattern can partially explain the response in the Pacific sector, while the poleward contraction of the atmospheric westerlies (see Figure 3.2c; L’Heureux and Thompson 2006) during a cold ENSO event can excite an Ekman response in all basins of the Southern Ocean.

Consistent with the existing literature (see, e.g. Yuan and Martinson 2000; Liu et al. 2002; Kwok and Comiso 2002; Lefebvre et al. 2004; Liu et al. 2004; Yuan 2004), we find that ENSO also drives a significant change in sea ice concentra-

tion in the southeastern Pacific and southwestern Atlantic Oceans (Figure 3.2i). During cold ENSO events, the PSA-driven cyclonic circulation anomaly in the atmosphere of the eastern Pacific (see, e.g. Figure 3.1, note that regression is on the standard ENSO index) advects anomalously cold air into the region over the Ross/Amundsen sector and warm air over the Bellingshausen/Weddell sector (Liu et al. 2004), creating anomalous heat fluxes in these regions which enhance and reduce sea ice concentrations. We also find small areas in the Atlantic and Indian sectors where ENSO has a significant impact on sea ice concentration (Figure 3.2i).

Chlorophyll concentrations throughout the Southern Ocean are significantly impacted by ENSO (Figure 3.2m). In the subtropical gyre of the Pacific, cold ENSO events are associated with lower than normal chlorophyll concentrations, whereas the subtropical gyres of the Atlantic and Indian basins experience increased chlorophyll during cold ENSO events. As biological activity in these subtropical regions is thought to be limited by macronutrients and stratification here is dominated by temperature (Pollard et al. 2002), the chlorophyll response in these regions can be explained by the SST response to ENSO (Figure 3.2f). Cold ENSO events are characterized by warm SST anomalies in the Pacific, driving an increase in stratification, an decrease in macronutrient supply to the surface, and a subsequent decrease in biological activity. In the subtropical Atlantic and eastern Indian basins, cold ENSO events are associated with colder than normal SST, weaker stratification, enhanced nutrient supply, and increased chlorophyll concentrations.

In the Subantarctic Zone (SAZ) of the South Atlantic, we find enhanced

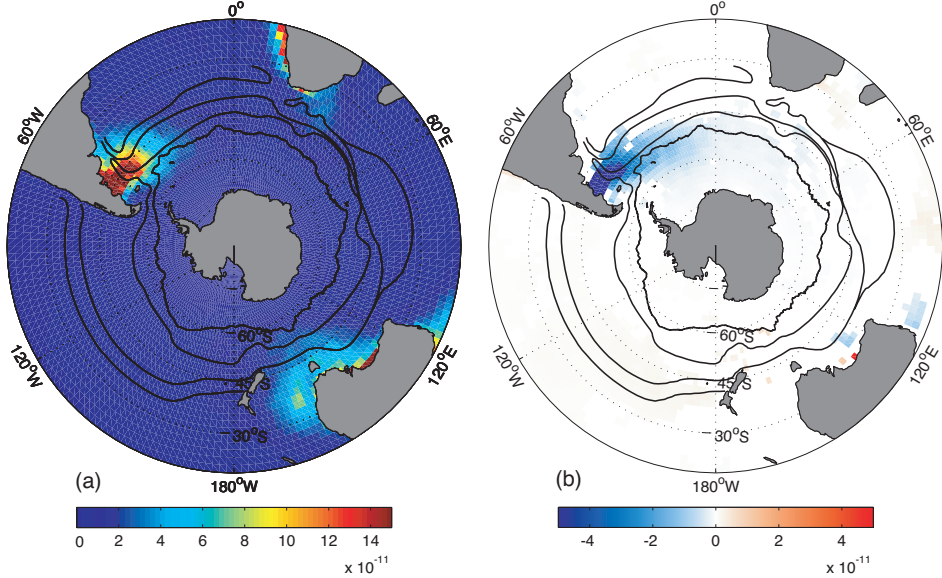


Figure 3.4: (a) Annual-mean dust deposition, and (b) regression of dust deposition anomalies onto the ENSO index ($\text{kg m}^{-2} \text{s}^{-1}$). Only those regressions whose correlations are significant at $>95\%$ are plotted in (b).

chlorophyll during cold ENSO events (Figure 3.2m). This is a region where chlorophyll concentrations are typically high, owing to the iron input to the surface ocean from aeolian dust deposition, shelf-basin mixing, and upwelling/entrainment (Moore and Abbott 2000). While a number of factors could be responsible for the ENSO-related variability in chlorophyll here, we investigate the possible role of changes in aeolian dust deposition. To do this, we use daily output from the Model of Atmospheric Transport and Chemistry which has been forced with NCEP reanalysis data from 1979-2004 and includes the Desert Entrainment and Deposition Model dust module (Mahowald et al. 2003). Daily dust deposition output from the model was averaged into 8-day periods to correspond to observations of chlorophyll. The 8-day deposition fields were then deseasonalized and detrended as above to create anomalies. Figure 3.4a shows annual-mean dust

dust deposition from 1997 to 2003. Dust deposition is high off the eastern coast of southern South America, owing to the large dust source in Patagonia (Gassó and Stein 2007). In fact a large portion of the iron supplied to the upper ocean in this region comes from dust deposition (Fung et al. 2000). We regress anomalies in dust deposition (1997-2003) from Mahowald et al. (2003) onto the standard ENSO index in Figure 3.4b, and find that cold ENSO events are associated with a significant enhancement in dust deposition off the Patagonia coast. During cold ENSO events, there is less rainfall in southeastern South America (Trenberth et al. 1998), and more dust input to the atmosphere (Mahowald et al. 2003). The anomalously high dust deposition during cold ENSO events therefore serves as one possible explanation for the higher than normal chlorophyll observed in this region.

The Antarctic Zone (AZ) is the only region that exhibits a statistically significant relationship between ENSO and chlorophyll (Table 3.2). Here, cold ENSO events are associated with increased chlorophyll near the Antarctic Peninsula and in the western Indian sector, and increased chlorophyll in the eastern Atlantic sector (Figure 3.2m). We suspect that some interaction between SAM and ENSO is driving these regions of significant correlation, as discussed next.

3.6 Discussion

While we have separately investigated the impact of SAM and ENSO on the Southern Ocean, it is important to note that SAM and ENSO are not linearly independent. ENSO creates unique patterns of variability in the Pacific sector of the Southern Ocean, but zonal wind anomalies associated with ENSO can also

project onto the SAM (L'Heureux and Thompson 2006). In the austral summer, nearly 25% of SAM variability can be explained by ENSO (L'Heureux and Thompson 2006), and the two year-round indices correlate at $r = -0.4$ (see, e.g. Figure 3.3). A large fraction of the anomalies in wind, SST, sea ice, and chlorophyll that are correlated with the SAM have an equal but opposite correlation with ENSO (compare second and third columns of Figure 3.2 and see Table 3.2).

In the previous chapter, we show that positive phases of the SAM are associated with lower than normal SST and elevated chlorophyll concentrations in the AZ. In the SAZ, we find decreased chlorophyll, and the STZ is characterized by warm SST and reduced chlorophyll concentrations. During positive SAM, the winds are stronger than normal over the AZ and PFZ, creating circulation anomalies which then impact surface temperature and biological activity. We attribute the AZ chlorophyll-SAM response to an increased upwelling of iron, the SAZ response to light limitation from deeper mixed layers, and the STZ response to decreased macronutrient supply from stronger stratification.

Cold ENSO events are similar to positive SAM events, in that they are both associated with a poleward contraction of the westerly winds (Figure 3.2b and c), indicating that we can expect a similar Southern Ocean circulation response to ENSO as to the SAM. The patterns and magnitude of the variance in both SST and sea ice concentration explained by the SAM and ENSO are rather similar (Figure 3.2e,f,h,i). The only exception to this is the subtropical Pacific SST, which has a more robust response to ENSO. It has been shown that the mechanisms which drive variability in Southern Ocean SST and sea ice concentration are similar for both SAM and ENSO (Ciasto and Thompson, in press; Verdy et al.

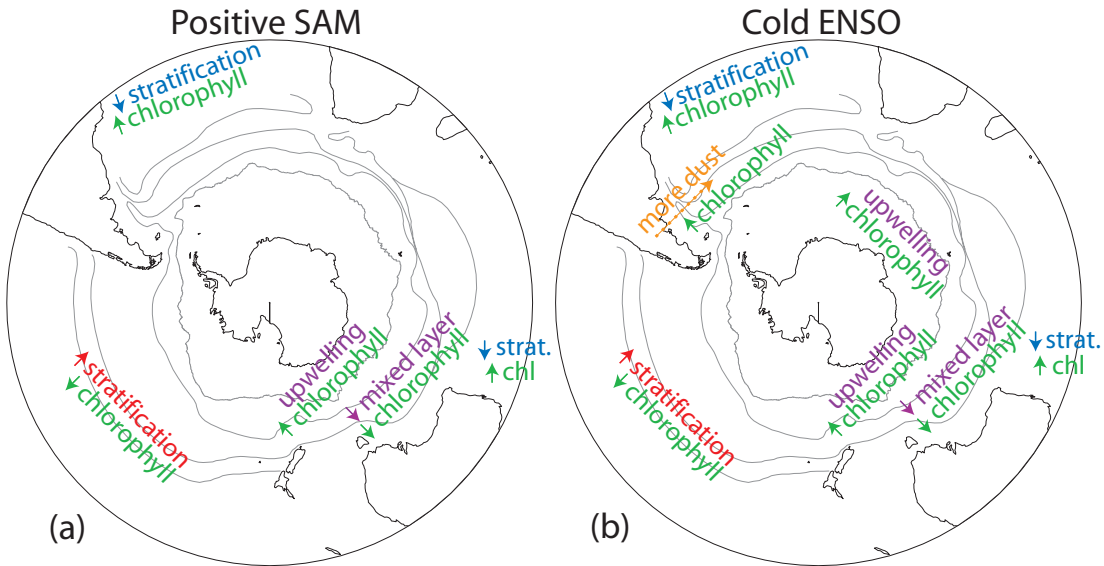


Figure 3.5: Schematic illustration of biological response to (a) positive SAM, and (b) cold ENSO events.

2006; Liu et al. 2004). This suggests that the mechanisms which drive variability in chlorophyll concentration are also similar between SAM and ENSO.

Many of the spatial patterns in Figure 3.2k appear again in Figure 3.2m. We summarize and interpret these chlorophyll responses to the SAM and ENSO in Figure 3.5. In the region south of Australia, for example, there is elevated chlorophyll in the AZ during positive SAM and cold ENSO events, where increased supply of iron to the surface waters from upwelling likely increases production. There is also a reduction in chlorophyll in the SAZ during positive SAM/cold ENSO, where increased convergence and deeper than normal mixed layers could limit the light available to phytoplankton. The subtropical Pacific is another region of decreased chlorophyll during both positive SAM and cold ENSO, as macronutrient supply gets cut off from the surface during times of stronger stratification.

There are a few places, however, where ENSO appears to have a significant

correlation with chlorophyll and SAM does not (Figure 3.5). In the Atlantic and western Indian sectors of the AZ, we find significant chlorophyll-ENSO correlations that are not shared by SAM. Upon closer inspection of Figure 2.1c from the previous chapter, we see that while similar SAM-chlorophyll relationships exist here, they are not strong enough to be considered statistically significant. A likely explanation for the correlation between ENSO and chlorophyll in the AZ is the enhanced upwelling of iron into this region, which could occur during both positive SAM and cold ENSO events. As the timescales of chlorophyll variability in this region are long (not shown), the higher correlations with ENSO here could also reflect the low frequency character of the index, as opposed to the high frequency character of the SAM (see, e.g. Figure 3.3e and f). In the SAZ of the western Atlantic, we also find significant chlorophyll-ENSO regressions that do not exist for SAM. As discussed previously, this chlorophyll response probably relates to a teleconnection pattern that is associated with ENSO and not with the SAM.

We conclude that SAM and ENSO both drive variability in the Southern Ocean. While SAM varies over shorter timescales than ENSO, the mechanisms by which they influence Southern Ocean circulation and biology appear to be very similar.

3.7 Conclusions

In conjunction with the results from the previous chapter, we have demonstrated that SAM and ENSO are both important contributors to the variability in the Southern Ocean. ENSO has a large impact on SST and sea ice concentration

variability in the Pacific sector, but SAM and ENSO both affect wind speed, SST, sea ice, and chlorophyll concentrations throughout most of the Southern Ocean. While the analysis in the remaining chapters of this dissertation focuses exclusively on the SAM impact in the Southern Ocean, this study suggests that Southern Ocean variability cannot be attributed solely to the SAM. These two large modes of variability can help us to understand a large fraction of the variance in the Southern Ocean, however more than half of the total variance is still unexplained by either phenomenon (see Table 3.2). This remaining variance could be related to small scale variability that is not coherent on the large scales investigated here.

Chapter 4

Enhanced CO₂ outgassing in the Southern Ocean from a positive phase of the Southern Annular Mode

4.1 Abstract

We investigate the interannual variability in the flux of CO₂ between the atmosphere and the Southern Ocean on the basis of hindcast simulations with a coupled physical-biogeochemical-ecological model with particular emphasis on the role of the Southern Annular Mode (SAM). The simulations are run under either pre-industrial or historical CO₂ concentrations, permitting us to separately investigate natural, anthropogenic, and contemporary CO₂ flux variability. We find large interannual variability ($\pm 0.19 \text{ PgC yr}^{-1}$) in the contemporary air-sea CO₂ flux from the Southern Ocean ($<35^\circ\text{S}$). 43% of the contemporary air-sea CO₂ flux variance is coherent with SAM, mostly driven by variations in the flux of natural CO₂, for which SAM explains 48%. Positive phases of the SAM are associated with anomalous outgassing of natural CO₂ at a rate of 0.1 PgC yr^{-1} .

per standard deviation of the SAM. In contrast, we find an anomalous uptake of anthropogenic CO₂ at a rate of 0.01 PgC yr⁻¹ during positive phases of the SAM. This uptake of anthropogenic CO₂ only slightly mitigates the outgassing of natural CO₂, so that a positive SAM is associated with anomalous outgassing in contemporaneous times. The primary cause of the natural CO₂ outgassing is anomalously high oceanic partial pressures of CO₂ caused by elevated dissolved inorganic carbon (*DIC*) concentrations. These anomalies in *DIC* are primarily a result of the circulation changes associated with the southward shift and strengthening of the zonal winds during positive phases of the SAM. The secular, positive trend in the SAM has led to a reduction in the rate of increase of the uptake of CO₂ by the Southern Ocean over the past 50 years.

4.2 Introduction

Variations in the oceanic sources and sinks of atmospheric CO₂ are an important contributor to the interannual variability in the atmospheric CO₂ growth rate (Bousquet et al. 2000; Peylin et al. 2005). Processes that regulate the exchange of CO₂ between the ocean and atmosphere are likely to change in a future characterized by global warming, leading to positive and negative feedbacks in the global climate system (Sarmiento et al. 1998; Joos et al. 1999; Matear and Hirst 1999; Plattner et al. 2001; Gruber et al. 2004). Studying the interannual variability in these processes over the last few decades and their impact on atmospheric CO₂ may help to determine the future evolution of atmospheric CO₂. Understanding the mechanisms leading to air-sea CO₂ flux variations is therefore a crucial, albeit not sufficient, condition to quantify the future behavior of the

global carbon cycle. Model estimates of global interannual air-sea CO₂ flux variations are on the order of $\pm 0.50 \text{ PgC yr}^{-1}$, and suggest that they mostly originate from the Tropical Pacific (LeQuéré et al. 2000; McKinley et al. 2004). Inversions of atmospheric CO₂ tend to agree with the model based results with regard to the magnitude of the variability in the Tropical Pacific (McKinley et al. 2004; Peylin et al. 2005), but tend to differ with regard to the magnitude of the extratropical variability in the air-sea CO₂ fluxes. Unfortunately, the observational coverage of measurements of the oceanic partial pressures of CO₂ is insufficient in most extratropical regions to establish the interannual variations in the air-sea CO₂ fluxes based on in situ data with very few exceptions (Gruber et al. 2002; Dore et al. 2003; Brix et al. 2004; Lefévre et al. 2004). Although ill constrained, the contribution from extratropical regions is likely non-negligible. In fact, a recent model study suggests that the Southern Ocean alone accounts for over 20% of the interannual CO₂ flux variability (Wetzel et al. 2005).

The unique physical oceanography of the Southern Ocean sets the stage for its important role in the global climate system. Atmospheric westerlies propel the strong eastward flow of the Antarctic Circumpolar Current (ACC), providing a pathway for the propagation of climatic signals from basin to basin. Westerlies also drive northward Ekman drift, creating the surface branch of a meridional overturning circulation, the Deacon Cell, that may be linked to the global thermohaline circulation (Rintoul et al. 2001). The rate of meridional overturning is critical to the processes regulating the exchange of CO₂ between the atmosphere and the Southern Ocean. Upwelling in the Antarctic Divergence exposes deep waters with elevated concentrations of dissolved inorganic carbon (*DIC*) to the

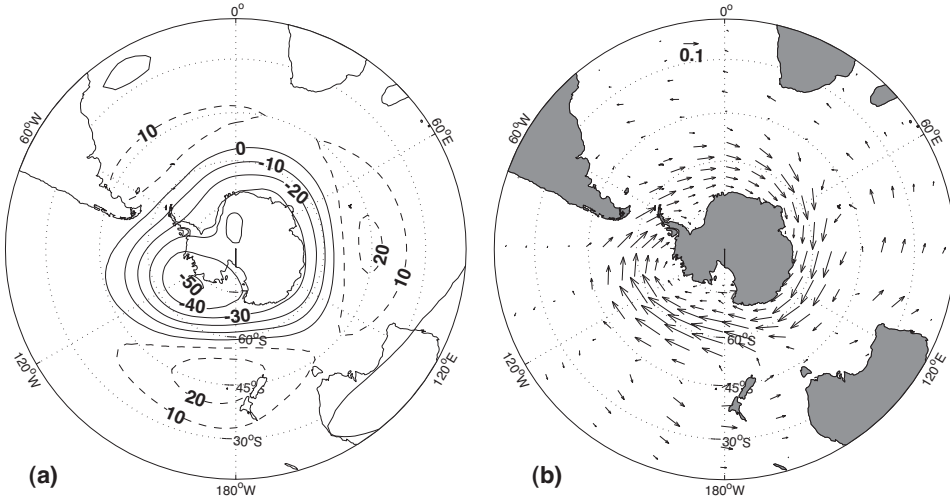


Figure 4.1: Regression of (a) 700 mb geopotential height anomalies (m), and (b) wind stress anomalies (dyne cm^{-2}) onto the standardized SAM index. Regressions for the zonal and meridional components of the wind stress were calculated separately. For clarity, arrows are only drawn at every other latitude and every fifth longitude point. Note scale arrow near the top of (b).

surface, leading to the ventilation of natural CO_2 to the atmosphere (Mikaloff-Fletcher et al. 2007; Toggweiler and Samuels 1993; Murnane et al. 1999). The natural CO_2 which is lost to the atmosphere originates as respired carbon from sinking particles, and is important for determining atmospheric CO_2 on longer timescales (Sarmiento and Toggweiler 1984; Siegenthaler and Wenk 1984). At the same time, approximately 40% of the global oceanic sequestration of anthropogenic CO_2 occurs on the downwelling side of the Deacon Cell (Sabine et al. 2004; Mikaloff-Fletcher et al. 2006), in association with the formation of mode and intermediate waters (McCartney 1982). Gruber et al. (submitted) estimate that this high rate of uptake of anthropogenic CO_2 has turned the Southern Ocean from a preindustrial source of CO_2 to the atmosphere to a net sink for atmospheric CO_2 , consistent with the new $p\text{CO}_2$ climatology of Takahashi et al. (in

preparation). Given the large exchange fluxes of both natural and anthropogenic CO₂, and the potential for sensitivity to future climate change (Sarmiento et al. 1998), it is pertinent to understand how this region responds to climate variability and how it might be affected by climate change.

Both observations (Lovenduski and Gruber 2005; Hughes et al. 2003; Liu et al. 2004) and models (Hall and Visbeck 2002; Oke and England 2004; Watterson 2000) have shown that most of the interannual climatic variability in the Southern Ocean is closely tied to the Southern Annular Mode (SAM), the dominant mode of atmospheric interannual variability in the extratropical circulation of the Southern Hemisphere (Thompson and Wallace 2000). The spatial pattern associated with the SAM represents a nearly zonally symmetric oscillation of pressure over the Pole and pressure over midlatitudes (Figure 4.1a). The SAM index is defined as the leading principal component of monthly geopotential height anomalies south of 20°S, such that positive SAM is associated with anomalously low pressure over the Pole. Such a positive SAM is also coincident with a poleward shift of the westerly winds (Figure 4.1b) (Hartmann and Lo 1998; Limpasuvan and Hartmann 1999; Lovenduski and Gruber 2005). Since air-sea CO₂ flux is directly influenced by wind speed, and wind anomalies can alter the circulation and biogeochemistry of the ocean, and hence the oceanic *p*CO₂, it is likely that wind anomalies associated with the SAM can impact the flux of CO₂ between the atmosphere and the Southern Ocean.

Here we use output from a hindcast simulation of a global ocean general circulation model with an embedded biogeochemical-ecological model to investigate the interannual variability in the flux of CO₂ between the atmosphere and the

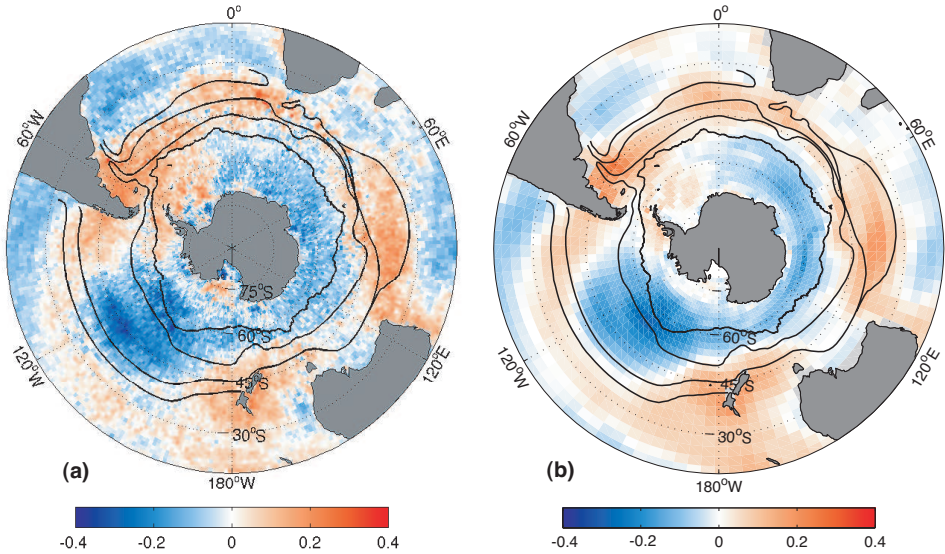


Figure 4.2: Regression of (a) observed SST anomalies, and (b) model SST anomalies from the historical simulation onto the standardized SAM index ($^{\circ}\text{C}$). Black contours mark the location of the Southern Ocean fronts. From pole to equator these fronts are: APF, SAF, SSTF, and NSTF.

Southern Ocean under contemporary conditions. We then separately investigate how much of this variability is driven by the air-sea flux of natural carbon, and how much by the flux of anthropogenic CO_2 . This separation is made by running the model using either a constant pre-industrial atmospheric CO_2 ($278 \mu\text{atm}$) or the time-varying historical atmospheric CO_2 record over the last 250 years as surface boundary conditions. The difference between these two runs is considered anthropogenic CO_2 , while the fluxes in the pre-industrial simulation are just that of natural carbon. Defined this way, the only factor driving the oceanic uptake of anthropogenic CO_2 is the anthropogenic perturbation of atmospheric CO_2 . The anthropogenic CO_2 uptake rate is then modified by variability and trends in ocean circulation, windspeed, and the surface ocean buffer factor (Gruber et al. 2004). In contrast, the air-sea exchange flux of natural carbon is not impacted

by changes in atmospheric CO₂, but responds to all climate variability induced changes of the relevant driving factors, such as windspeed, temperature, salinity, ocean circulation, and ocean biology. Trends in the physical forcing, whether of anthropogenic origin or not, will impact both anthropogenic and natural CO₂ fluxes. However, as we will see, it is primarily the natural CO₂ fluxes that are responding to climate variability and change. Additionally, we quantify the relationship between anomalies in the air-sea flux of contemporary, natural, and anthropogenic CO₂ and the SAM and analyze the mechanisms responsible for CO₂ flux variability associated with the SAM.

Using similar approaches, but employing different ocean circulation and biogeochemical models, two recent studies have also begun to explore the relationship between the SAM and Southern Ocean CO₂ fluxes. Lenton and Matear [submitted manuscript] used the ocean component of the CSIRO model with similar forcing, but undertook just a historical simulation. As a result, they were only able to investigate the variability of the contemporary air-sea CO₂ flux, while our running of both historical and pre-industrial simulations permits us to separately determine the impact of the SAM on natural and anthropogenic CO₂ fluxes. Wetzel et al. (2005) also explored air-sea CO₂ flux variability in the Southern Ocean and its connection to SAM. Similar to Lenton and Matear, they found anomalous outgassing of CO₂ during positive phases of SAM. Wetzel et al. (2005) also noted an outgassing trend in the air-sea CO₂ flux from the Southern Ocean, and suggested that the trend was likely related to a trend in the SAM. This positive trend in the SAM over the past few decades (Thompson et al. 2000; Thompson and Solomon 2002) may itself be linked to climate change at high latitudes (Carril

et al. 2005). Here, we extend on these two studies with a more in-depth analysis, and use a more realistic ecosystem model coupled to an advanced global ocean general circulation model. We confirm the basic findings of these prior studies in that positive SAM leads to an anomalous outgassing, but demonstrate also the importance of the differential impact of SAM on natural and anthropogenic CO₂. We also elucidate that the main driver for the changes are alterations in the meridional overturning circulation, as suggested by Lovenduski and Gruber (2005).

4.3 Methods

We determine the interannual variability of the air-sea CO₂ fluxes in the Southern Ocean on the basis of hindcast simulations using a state-of-the-art biogeochemical-ecological model that has been coupled to the Parallel Ocean Program (POP) ocean general circulation model. POP is a level-coordinate, hydrostatic, primitive equation model integrated here with a resolution of 3.6° in longitude, 0.8° to 1.8° in latitude, and 25 vertical levels (Yeager et al. 2006). The effects of eddy transport are parameterized according to Gent and McWilliams (1990). The biogeochemical-ecological model is taken from the NCAR global Community Climate System Model (CCSM) and consists of a multiple phytoplankton functional group model for the euphotic zone processes, and a relatively simple biogeochemical model for the aphotic zone processes. This model is comprised of several nutrient, phytoplankton, zooplankton, and detritus components, and contains complex ecosystem parameterizations, including an iron cycle. The model equations are identical to those reported for the 3-D implementation of Moore et al.

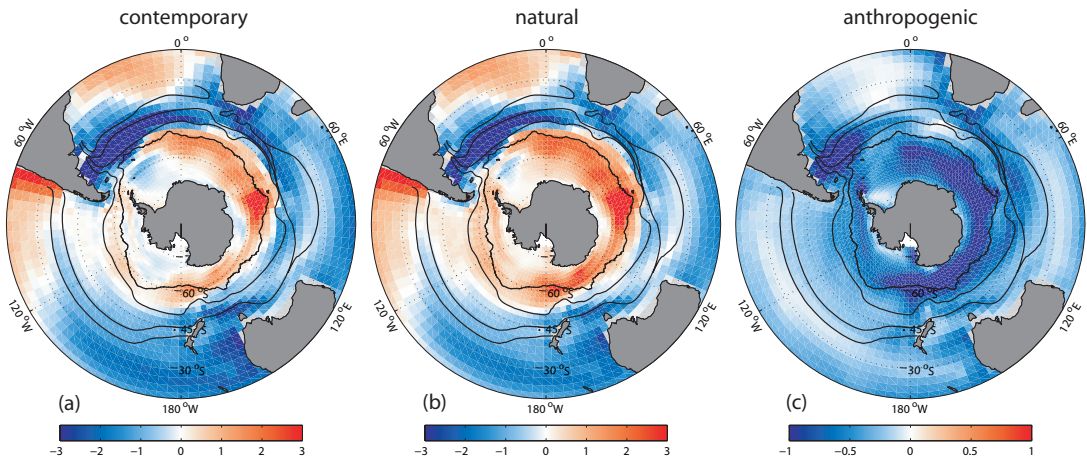


Figure 4.3: Annual-mean air-sea flux of (a) contemporary CO₂ (natural + anthropogenic CO₂), (b) natural CO₂, and (c) anthropogenic CO₂ ($\text{mol m}^{-2} \text{ yr}^{-1}$). The fluxes have been averaged using output from the historical simulation for (a), pre-industrial simulation for (b) and from their difference for (c). Positive fluxes indicate ocean outgassing. Note difference in scale for the anthropogenic flux.

(2004) with two important modifications as documented in more detail in Moore et al. (2006). First, water column denitrification has been added to the model in order to close the global nitrogen cycle. Second, a number of the parameters associated with the model iron dynamics and scavenging have been adjusted to improve the simulated dissolved iron fields (see Table 1 of Moore et al. (2006)).

The coupled physical-biogeochemical-ecological model is first spun up to an approximate cyclostationary state with prescribed repeating annual cycles of physical forcing and dust deposition and a pre-industrial atmospheric CO₂ mixing ratio of 278 ppm. Two separate hindcast simulations are then performed with the model. In the first, atmospheric CO₂ is held at a constant pre-industrial value of 278 ppm, and in the second, the model is run using the measured and reconstructed evolution of atmospheric CO₂ from 1765 to 2004 as a boundary condition. We refer to the former as the *pre-industrial simulation* and the latter

as the *historical simulation*. The CO₂ fluxes from the pre-industrial simulation are driven by the cycling of *natural CO₂*, while the CO₂ fluxes from the historical run represent the sum of natural and *anthropogenic CO₂*. We determine the flux of anthropogenic CO₂ by subtracting the CO₂ flux in the pre-industrial simulation from the CO₂ flux in the historical simulation. In doing so, we assume that variations in the natural carbon cycle have no influence on the uptake of anthropogenic CO₂. This assumption is not without caveats, as variations in the natural carbon cycle change the buffer (Revelle) factor of the ocean (Sarmiento and Gruber 2006, chapter 8), and hence can alter the ocean's capacity for taking up anthropogenic CO₂ from the atmosphere. However, since model simulations that include/exclude an active natural carbon cycle give very similar results with regard to the uptake of anthropogenic CO₂ (Watson and Orr 2003), we judge the impact of the interaction between the natural and anthropogenic carbon cycle to be small. Both the historical and pre-industrial simulations are brought from the initial cyclo-stationary state (1765) to 1957 using repeating annual cycles of physical forcing following Doney et al. (in press). Then, both simulations are forced with 6-hourly heat, monthly freshwater, and 6-hourly momentum fluxes computed using bulk transfer formula and surface atmosphere data from the National Center for Environmental Prediction/National Center for Atmospheric Research (NCEP/NCAR) reanalysis (Kalnay et al. 1996), as well as satellite data products including daily Goddard Institute for Space Studies radiation and Special Sensor Microwave/Imager monthly ice fraction from 1958 through 2004 (Large and Yeager 2004). There is a repeating annual cycle of surface dust flux (Mahowald et al. 2003) in both simulations. Gas exchange is parameterized using

a quadratic wind speed relationship as described by Wanninkhof (1992).

After analyzing the modeled mean state, we conduct statistical analyses on monthly anomalies of model output from 1958 through 2004. Monthly anomalies represent what remains after the climatological mean seasonal cycle and linear trend have been removed from the output at each location and depth. Seasonal cycles were calculated by binning all output into 12 monthly bins and then taking the average. Linear trends were removed from all of the pre-industrial output, as well as most of the historical output. The trends removed from historical air-sea CO₂ fluxes, surface ocean *pCO₂*, and *DIC* were determined by finding the least-squares fit to the data as a linear function of the historical atmospheric CO₂ curve. With the exception of Table 4.1, we ignore the modeled drift in air-sea CO₂ flux. We correlate and regress anomalies onto a standardized SAM index, using the method of Bretherton et al. (1999) to determine the statistical significance of correlation coefficients in the presence of autocorrelation.

Statistical analyses are performed on both a point-by-point and regional average basis. In the case of the regional averages, the Southern Ocean is divided into four distinct zones, whose boundaries are well-known fronts. These fronts represent steep gradients in vertical structure, temperature, salinity, and nutrient concentration. The fronts we use here were derived from satellite sea surface temperature (SST) data (Moore et al. 1999), as well as data collected during meridional section cruises (Belkin and Gordon 1996). It is unlikely that this will lead to artifacts in the analysis, as the position of the observed fronts nearly corresponds to those derived from the model (not shown). For the purposes of our analysis, we assume the fronts are stationary. The Antarctic Zone (AZ) is

Table 4.1: Annual-mean air-sea fluxes of modeled contemporary, natural, and anthropogenic CO₂ (Pg C yr⁻¹). Flux estimates from ocean inversions and observations are shown for comparison. Positive values indicate ocean outgassing. Inversion estimates are taken from Mikaloff-Fletcher et al. (2006) and Mikaloff-Fletcher et al. (2007), while observational estimates are from Takahashi et al. (in preparation).

Region	Latitudes	Contemporary			Natural		Anthropogenic	
		model ^{a,b}	inversion	observed	model ^a	inversion	model ^b	inversion
S. Atl, Low-Lat	18°S-31°S	0.04	-0.01 ± 0.01	0.03	0.08	0.02 ± 0.01	-0.03	-0.02 ± 0.01
S. Atl, Mid-Lat	31°S-44°S	-0.34	-0.16 ± 0.05	-0.16	-0.26	-0.11 ± 0.05	-0.07	-0.05 ± 0.02
S. Sub-Polar Atl	44°S-58°S	-0.05	0.00 ± 0.08	-0.13	-0.02	0.11 ± 0.05	-0.08	-0.11 ± 0.07
S. Ocean	S. of 58°S	0.08	-0.20 ± 0.11	0.01	0.25	0.04 ± 0.04	-0.19	-0.24 ± 0.10
S.W. Pac, Mid-Lat	18°S-44°S	-0.58	-0.44 ± 0.10	-0.36	-0.46	-0.35 ± 0.09	-0.13	-0.09 ± 0.04
S.E. Pac, Mid-Lat	18°S-44°S	0.09	-0.02 ± 0.03	0.04	0.15	-0.01 ± 0.03	-0.04	-0.02 ± 0.01
S. Sub-Polar Pac & Ind	44°S-58°S	0.10	-0.14 ± 0.15	-0.31	0.27	0.25 ± 0.09	-0.23	-0.39 ± 0.12
S. Ind, Mid-Lat	18°S-44°S	-0.52	-0.46 ± 0.09	-0.46	-0.38	-0.22 ± 0.06	-0.16	-0.24 ± 0.07
<i>Sum of Regions</i>		-1.18	-1.43 ± 0.25	-1.34	-0.37	-0.27 ± 0.17	-0.93	-1.16 ± 0.19

^a Regional estimates have been adjusted for a global -0.52 Pg C yr⁻¹ drift.

^b Model estimates of contemporary and anthropogenic fluxes represent an average from 1990 to 2000.

defined as the region south of the Antarctic Polar Front (APF) (Moore et al. 1999). The Polar Frontal Zone (PFZ) is the region between the APF and the Subantarctic Front (SAF), and the Subantarctic Zone (SAZ) is the region between the SAF and the South Subtropical Front (SSTF). The Subtropical Zone (STZ) is bordered by the SSTF and the North Subtropical Front (NSTF) (Belkin and Gordon 1996). Anomaly time series of output from each region are created by averaging the anomalies of all points within the region.

The SAM index used here is the first principal component of the monthly 700 mb geopotential height anomalies south of 20°S from 1958-2004 obtained from the NCEP/NCAR reanalysis (Figure 4.1a). The index is standardized by subtraction of the mean and division by the standard deviation. Since it is believed that the SAM has a relatively weak seasonality (Hall and Visbeck 2002; Hartmann and Lo 1998), we use year-round data to construct the index. Our index correlates with the monthly SAM index from the NOAA Climate Prediction Center (1979-2004) [<http://www.cpc.ncep.noaa.gov>] at $r=0.97$.

4.4 Model evaluation

The successful modeling of the interannual and long-term variations in the air-sea CO₂ fluxes requires a well evaluated model, whose strengths and weaknesses are well established. Due to the sparseness of carbon related observations in the Southern Ocean, and the importance of ocean physics in determining our results, we limit the evaluation to the interannual variations of a few physical parameters (SST, sea-surface height), and the annual mean air-sea CO₂ fluxes from ocean inversion models and surface $p\text{CO}_2$ observations.

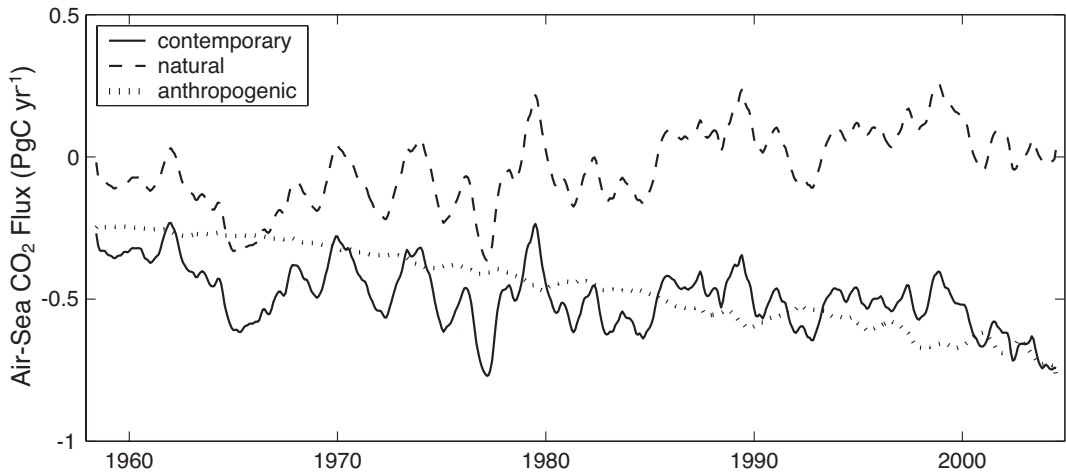


Figure 4.4: Mean Southern Ocean ($<35^{\circ}\text{S}$) air-sea CO_2 flux, smoothed with an 12-month running average (PgC yr^{-1}). Negative fluxes indicate ocean uptake.

The SST in the physical model and in the real ocean respond in a similar way to anomalous surface forcing associated with the SAM. To compare the two, we use satellite observations of monthly averaged SST from AVHRR Oceans Pathfinder (versions 4.1 and interim 4.1) on a 9 km grid from 1985-2003 [<http://podaac.jpl.nasa.gov>]. Anomalies in SST were interpolated to a 1° grid, and surface temperature anomaly time series from the model were sampled to match the months of available SST data. Figure 4.2 shows the regression of the observed and modeled surface temperature anomalies onto the SAM index. The two regression patterns are nearly identical, indicating that the modeled SST response to the SAM compares well with the observed response. To illustrate this point further, we calculated the regression coefficients of the regional anomaly time series in both observed and modeled surface temperature with the SAM (not shown). The regression coefficients are indistinguishable in the AZ and PFZ, but there are small biases in the model regressions in the SAZ and STZ.

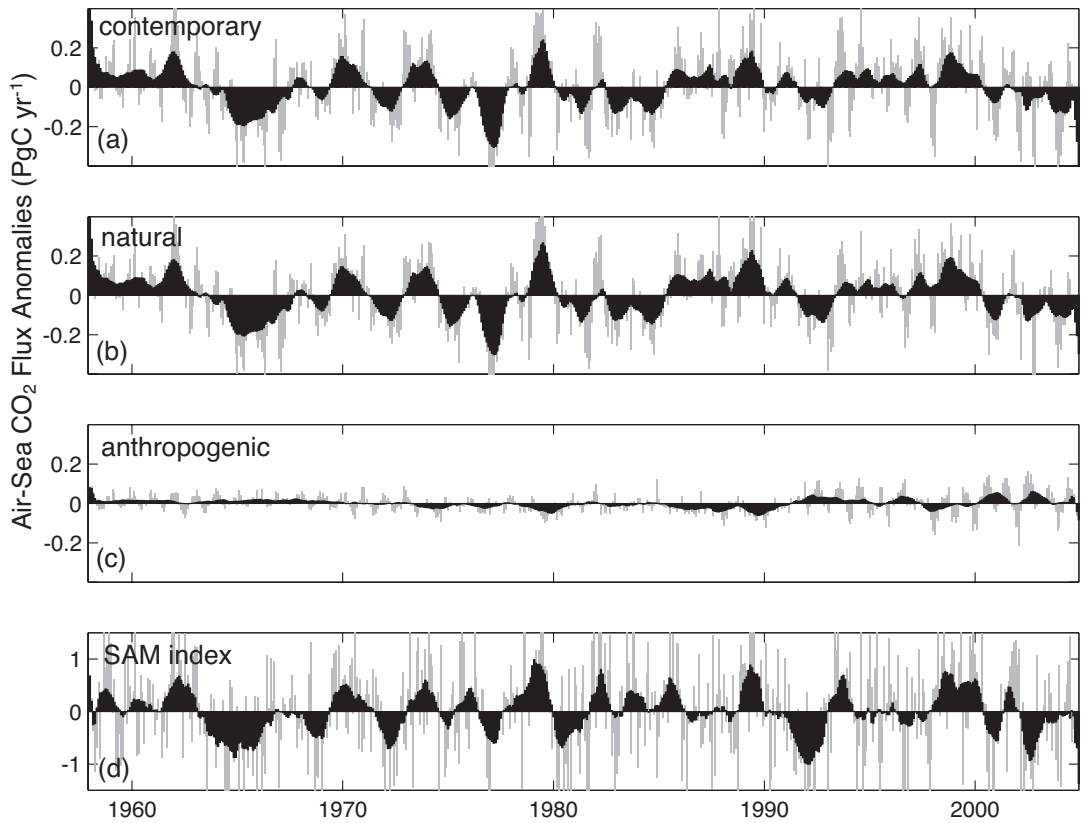


Figure 4.5: Southern Ocean air-sea flux anomalies of (a) contemporary, (b) natural, and (c) anthropogenic CO₂ (PgC yr⁻¹). (d) Standardized SAM index used in this study. Each time series has been smoothed with a 12-month running average, with the monthly time series displayed behind in gray. Positive fluxes indicate ocean outgassing.

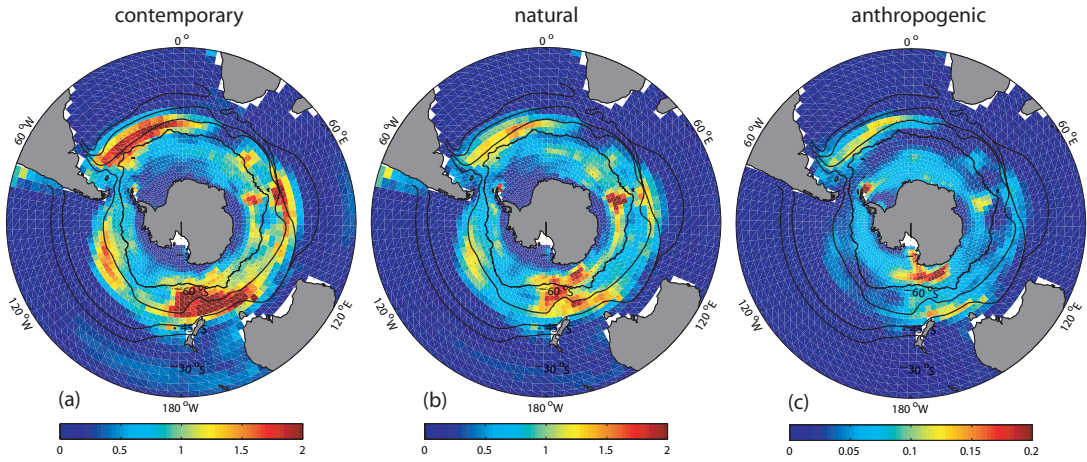


Figure 4.6: Variance of air-sea flux anomalies of (a) contemporary, (b) natural, and (c) anthropogenic CO_2 ($\text{mol m}^{-2} \text{yr}^{-1}$) 2 . Note that the scale of (c) is ten times smaller than that used in (a) and (b).

One possible cause for this offset is that while the observations represent the skin temperature of the ocean, temperature in the first layer of the model represents an average over the top 8 m. Another possible model bias is the lack of explicit consideration for the role of eddies, which are particularly abundant in the SAZ and STZ.

Similar success is found in the model’s ability to simulate ship-based heat content and ship and satellite-based sea-surface height variability (see Doney et al., in press), although they describe results from an earlier version of the POP model.

The coupled ocean physical-biogeochemical-ecological model reproduces quite successfully the annual mean air-sea CO_2 flux patterns in the Southern Ocean, as estimated by ocean inversion models and observations. Figure 4.3 shows the annual- mean contemporary (1990-2000), natural (1958-2000), and anthropogenic (1990-2000) air-sea CO_2 fluxes from the model, with positive fluxes into the at-

Table 4.2: The relationship between spatially-integrated ($<35^{\circ}\text{S}$) air-sea CO_2 flux anomalies and the standardized SAM index.

Quantity	Contemporary	Natural	Anthropogenic
<i>Regressions PgC yr⁻¹</i>			
Regression with SAM	0.09	0.10	-0.01
Smoothed Regression ^a	0.16	0.18	-0.02
Lag-1 Regression ^b	0.08	0.08	0
<i>Correlations (r)</i>			
Correlation with SAM	0.46	0.56	-0.28
Smoothed Correlation ^a	0.66	0.69	-0.35
Lag-1 Correlation ^b	0.42	0.47	-0.09

^a A 12-month running average was used.

^b The SAM leads the CO_2 fluxes by one month, without smoothing.

mosphere. The contemporary and natural CO_2 fluxes are that of outgassing in the region south of $\sim 55^{\circ}\text{S}$, while the mode water formation regions between ~ 40 - 55°S are regions of contemporary and natural CO_2 uptake. Anthropogenic CO_2 is everywhere being taken up by the Southern Ocean in the annual-mean, with most of the uptake occurring in the upwelling regions of the AZ and the mode water formation regions in the Atlantic and Indian basins. These patterns of contemporary, natural, and anthropogenic uptake and outgassing agree with inverse model estimates from Mikaloff-Fletcher et al. (2006) and Mikaloff-Fletcher et al. (2007) and with observed estimates from Takahashi et al. (in preparation) in the Southern Ocean regions used for this study (Table 4.1). While flux estimates may differ in the individual regions, the fluxes integrated over the entire Southern Ocean agree to within the uncertainties. Global estimates of air-sea CO_2 flux from this model are also well matched with inversion estimates and observations (not shown), particularly in terms of anthropogenic CO_2 , whose annual-mean modeled global uptake (1990-2000) is 1.98 PgC yr^{-1} , in agreement with a large range of independent estimates (as summarized by Gruber et al., submitted).

From these comparisons, we conclude that the coupled model demonstrates reasonable skill in its representation of the mean state and how this mean state is perturbed by interannual variations in surface forcing. This gives us some confidence in the modeled air-sea CO₂ flux variability, discussed next.

4.5 Variability of air-sea CO₂ fluxes

The timeseries of the Southern Ocean (< 35°S) integrated air-sea CO₂ fluxes in Figure 4.4 reveal a positive trend (less oceanic uptake with time) for natural CO₂, while the flux of anthropogenic CO₂ shows a strong negative trend (more oceanic uptake with time). The latter is expected as it reflects the oceanic response to increased atmospheric CO₂ concentration in the historical run, while it has been proposed that the former is due to a trend in the SAM index (Wetzel et al. 2005), as discussed in more detail below. The anthropogenic CO₂ trend exceeds that for natural CO₂, so that the contemporary air-sea flux also exhibits a negative trend. With regard to variations around these trends, Figure 4.4 suggests that most of the contemporary flux variability originates from variability in natural rather than anthropogenic CO₂. We first investigate the variability by focusing our analysis on model output that has been both deseasonalized and detrended, and return to the trends at the end.

The contemporary and natural air-sea CO₂ flux anomalies shown in Figure 4.5 exhibit large variability for the Southern Ocean: ±0.19 PgC yr⁻¹ and ±0.18 PgC yr⁻¹, respectively (1σ). These flux variances are substantially larger than those obtained previously for the Southern Ocean from ocean model simulations (e.g. ±0.1 PgC yr⁻¹ from Peylin et al. (2005) and ±0.05 PgC yr⁻¹ from Wetzel et al.

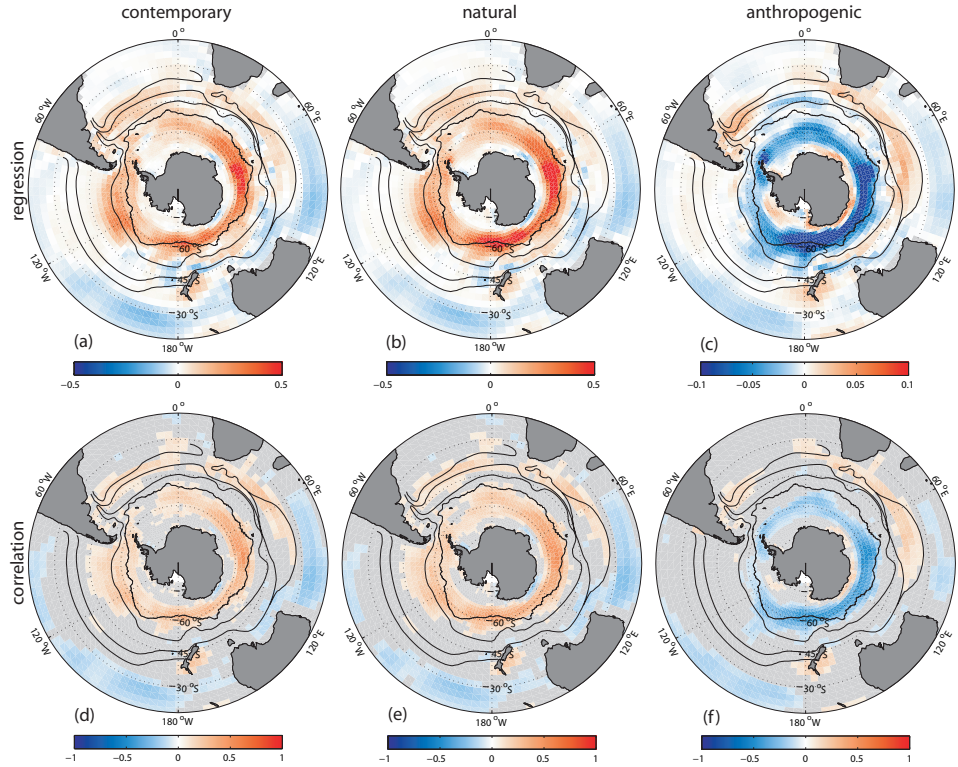


Figure 4.7: (a-c) Regression ($\text{mol m}^{-2} \text{ yr}^{-1}$), and (d-f) correlation of (a and d) contemporary, (b and e) natural, and (c and f) anthropogenic air-sea CO_2 flux anomalies with the SAM index. Regression coefficients correspond to one standard deviation change in the SAM index. Only those correlation coefficients with significance $\geq 95\%$ are shown. Positive fluxes indicate ocean outgassing. Note that the scale of (c) is 20% of (a) and (b).

(2005)). The model simulated contemporary and natural CO₂ flux variability from the Southern Ocean accounts for 30% of the global variance in these fluxes, which is in line with the estimated contribution from the Southern Ocean in other models (Wetzel et al. 2005; LeQuéré et al. 2000). The contemporary and natural monthly time series are well correlated ($r=0.96$), and exhibit similar spatial patterns of variance (Figure 4.6). In contrast, interannual variability in the air-sea flux of anthropogenic CO₂ does not exhibit high correlations with either contemporary or natural flux anomalies and is considerably smaller(± 0.05 Pg C yr⁻¹ (1σ), Figure 4.6). As atmospheric CO₂ concentrations grow throughout the simulation, variability in the anomalous anthropogenic CO₂ fluxes increases slightly.

Variance in the CO₂ flux anomalies is elevated in the region south of $\sim 45^{\circ}$ S (Figure 4.6), where the SAM is likely to have an influence on air-sea flux variability. Indeed, there is a clear connection between both the contemporary and natural air-sea CO₂ flux variability in the Southern Ocean ($<35^{\circ}$ S) and the SAM (Figure 4.5). The SAM explains 21% and 31% (r^2) of the variance in the contemporary and natural CO₂ flux anomalies, respectively (Table 4.2). When the time series are filtered with a 12-month running mean, the SAM explains 43% (r^2) of the variance in the contemporary CO₂ flux anomalies and 48% of that for natural CO₂ (Table 4.2). This implies that their relationship is stronger at lower frequencies. When the SAM leads the contemporary and natural CO₂ flux anomalies by one month (lag 1), the correlation with the SAM remains high (Table 4.2), suggesting that any anomalous contemporary or natural CO₂ flux linked to the SAM can persist for at least one month. In the rest of this paper, however,

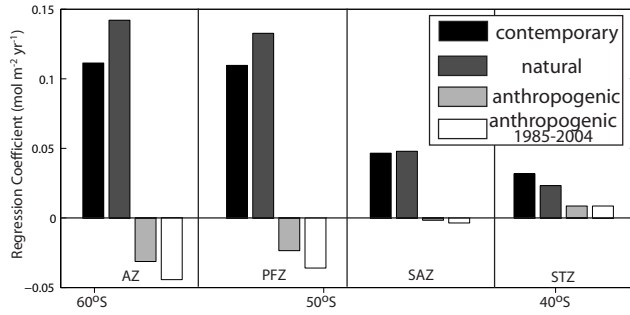


Figure 4.8: The regression coefficient of the SAM index with the regionally averaged time series of the air-sea flux anomalies of contemporary, natural, and anthropogenic air-sea CO_2 ($\text{mol m}^{-2} \text{yr}^{-1}$). Regression coefficients of anthropogenic CO_2 flux anomalies from the last 20 years (1985–2004) with the SAM are also plotted. Regression coefficients correspond to one standard deviation change in the SAM index. All regressions are statistically significant at >95%, with the exception of the anthropogenic coefficients in the SAZ.

we focus only on the monthly relationship at zero lag. Anthropogenic CO_2 flux anomalies have a weaker relationship with the SAM when spatially-integrated over the Southern Ocean (Table 4.2), although we will see next that climate variations associated with the SAM can slightly change the rate of anthropogenic CO_2 uptake.

Positive phases of the SAM are associated with significant anomalous outgassing of both contemporary and natural CO_2 throughout a large fraction of the Southern Ocean, as revealed by Figure 4.7. When integrated over the region south of 35°S , the rates of anomalous outgassing during a $+1\sigma$ SAM are 0.09 and 0.10 PgC yr^{-1} for contemporary and natural CO_2 , respectively (Table 4.2). In contrast, positive phases of the SAM are associated with small, but significant uptake of anthropogenic CO_2 in the same region, where the rate of anomalous uptake during a $+1\sigma$ SAM is 0.01 PgC yr^{-1} (Table 4.2). Anomalies in the outgassing and uptake stand out most clearly in the region south of 55°S , where the

regression coefficients are nearly zonally symmetric. However, regionally averaged time series of contemporary, natural, and anthropogenic CO₂ flux anomalies have strong relationships with the SAM in all four regions of the Southern Ocean, as demonstrated in Figure 4.8. Contemporary CO₂ outgassing is enhanced by 28% in the AZ and 33% in the PFZ during positive SAM, where enhanced outgassing of natural CO₂ is only slightly mitigated by enhanced uptake of anthropogenic CO₂. In the SAZ and STZ, positive phases of the SAM are associated with a reduction of contemporary CO₂ uptake. This reduction is mostly driven by the natural CO₂ response, as the anthropogenic response is small and only significant in the STZ (Figure 4.8). We find a larger anomalous anthropogenic CO₂ uptake in the AZ and PFZ during positive SAM over the last 20 years of the simulation (Figure 4.8), suggesting that the mitigating role of this component could become more important in the future.

4.6 Causes of the variability

In order to ascertain the mechanisms governing the contemporary CO₂ flux anomalies during positive SAM, it is most insightful to investigate the flux anomalies of natural and anthropogenic CO₂ separately. We focus first on the natural CO₂ flux anomalies by performing post-processing calculations on monthly output, and then briefly study the anthropogenic CO₂ flux anomalies.

We investigate the mechanisms responsible for the anomalous natural air-sea CO₂ flux during positive SAM by considering the total derivative of the air-sea CO₂ flux. As the model uses a standard bulk parameterization for the computation of this flux, the parameters to be considered are the gas exchange

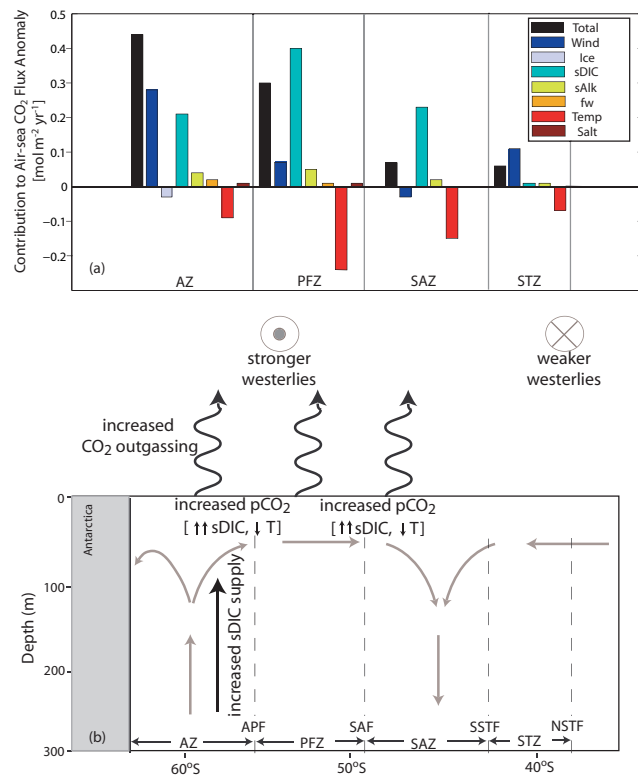


Figure 4.9: (a) Contribution to the air-sea CO_2 flux anomaly, ΔF , as in Equation 4 ($\text{mol m}^{-2} \text{yr}^{-1}$). (b) Schematic illustration of the upper ocean response to a positive phase of the SAM in the pre-industrial simulation.

coefficient (modeled as a function of windspeed (WS), temperature (T), and salinity (S)), the sea ice fraction (Ice), and surface ocean $p\text{CO}_2$ ($p\text{CO}_2^{oc}$). Here, we can neglect variations in atmospheric pressure and $p\text{CO}_2$ as it is assumed constant in the preindustrial simulation. Furthermore, variations in temperature and salinity have a relatively small impact on the gas exchange coefficient, so that we consider only the impact of windspeed. This yields for the relative contribution of each parameter to the anomalous air-sea CO_2 flux in each Southern Ocean region, ΔF ,

$$\Delta F = \frac{\partial F}{\partial WS} \Delta WS + \frac{\partial F}{\partial Ice} \Delta Ice + \frac{\partial F}{\partial p\text{CO}_2^{oc}} \Delta p\text{CO}_2^{oc}, \quad (4.1)$$

where $\frac{\partial F}{\partial WS}$, $\frac{\partial F}{\partial Ice}$, and $\frac{\partial F}{\partial p\text{CO}_2^{oc}}$ are determined from the model equations and mean values in each region. ΔWS and ΔIce are the differences of the mean wind speed and ice fraction, respectively, during a one standard deviation positive phase of the SAM and their mean values. The contribution to $\Delta p\text{CO}_2^{oc}$ is further decomposed into contributions from DIC , alkalinity (Alk), temperature, and salinity

$$\begin{aligned} \Delta p\text{CO}_2^{oc} = & \frac{\partial p\text{CO}_2^{oc}}{\partial DIC} \Delta DIC + \frac{\partial p\text{CO}_2^{oc}}{\partial Alk} \Delta Alk \\ & + \frac{\partial p\text{CO}_2^{oc}}{\partial T} \Delta T + \frac{\partial p\text{CO}_2^{oc}}{\partial S} \Delta S. \end{aligned} \quad (4.2)$$

As changes in DIC and Alk and hence changes in $p\text{CO}_2$ can be driven by variations in freshwater fluxes (Δfw) (see e.g. Keeling et al. (2004)) as well as by variations in ocean internal biogeochemical processes and transport/mixing, it is useful to separate the two mechanisms. We achieve this by expanding the

Table 4.3: Estimated contributions to the air-sea CO₂ flux anomalies, ΔF , as in Equation 4.3 [mol m⁻² yr⁻¹]. Positive fluxes are to the atmosphere. Σ is the sum of all seven terms, and ΔF_{mod} is the modeled anomaly in F during positive SAM.

Quantity	AZ	PFZ	SAZ	STZ
<i>Individual Terms</i>				
$\frac{\partial F}{\partial WS} \Delta WS$	0.28	0.07	-0.03	0.11
$\frac{\partial F}{\partial Ice} \Delta Ice$	-0.03	0	0	0
$\frac{S}{S_0} \frac{\partial F}{\partial DIC} \Delta sDIC$	0.21	0.40	0.23	0.01
$\frac{S}{S_0} \frac{\partial F}{\partial Alk} \Delta sAlk$	0.04	0.05	0.02	0.01
$\frac{\partial F}{\partial fw} \Delta fw$	0.02	0.01	0	0
$\frac{\partial F}{\partial T} \Delta T$	-0.09	-0.24	-0.15	-0.07
$\frac{\partial F}{\partial S} \Delta S$	0.01	0.01	0	0
<i>Sum of Terms Versus Modeled</i>				
Σ	0.44	0.30	0.07	0.06
ΔF_{mod}	0.25	0.21	0.09	-0.03

total derivatives and introducing salinity-normalized DIC ($sDIC$) and salinity normalized Alk ($sAlk$) (see Appendix A for more details). Substituting (4.2) and (A.1- A.3) into (4.1) yields,

$$\begin{aligned} \Delta F = & \frac{\partial F}{\partial WS} \Delta WS + \frac{\partial F}{\partial Ice} \Delta Ice + \frac{S}{S_0} \frac{\partial F}{\partial DIC} \Delta sDIC \\ & + \frac{S}{S_0} \frac{\partial F}{\partial Alk} \Delta sAlk + \frac{\partial F}{\partial fw} \Delta fw \\ & + \frac{\partial F}{\partial T} \Delta T + \frac{\partial F}{\partial S} \Delta S, \end{aligned} \quad (4.3)$$

whose individual terms are shown in Table 4.3 and Figure 4.9a.

The analysis of the total derivative of the air-sea flux of natural CO₂ during

a positive phase of SAM (Table 4.3, Figure 4.9a) demonstrates that variations in $sDIC$ and/or windspeed tend to dominate the overall response, and that their contribution is generally countered by opposing tendencies arising from temperature variations (Doney et al. 2006). The contribution of the other terms, such as $sAlk$, sea-ice, fw , and salinity is comparatively small. Windspeed tends to dominate in the Antarctic Zone (AZ) and the Subtropical Zone (STZ). The flux in the AZ is especially sensitive to wind speed changes, and the AZ experiences a large anomaly in wind speed during positive SAM. In the STZ, however, $\frac{\partial F}{\partial WS}$ is negative, so that a decrease in wind speed during positive SAM leads to anomalous outgassing. The contribution from $sDIC$ dominates in the Polar Frontal Zone (PFZ) and the Subantarctic Zone (SAZ), and plays a secondary role in the AZ. During positive SAM, we find increased $sDIC$ in the AZ, PFZ, and SAZ (Figure 4.10a, Table 4.4), leading to considerable $\Delta sDIC$ values in these regions. Temperature plays a secondary, but important role in mitigating the outgassing in both the PFZ and SAZ, where positive SAM leads to colder than normal surface temperatures (Figure 4.2), and hence large negative ΔT values.

While our analysis of the CO_2 derivative offers a simple way to understand the anomalous outgassing, we find a slight discrepancy between the sum of terms, Σ , and the modeled anomaly in F during positive SAM, ΔF_{mod} (Table 4.3, last two rows). The approximations used in the pCO_2 calculations (see (A.4)-(A.9)), or the possible cross-correlations among the variables may lead to imprecise results in some of the regions.

Given the importance of $sDIC$ variations for causing surface pCO_2^{oc} and air-sea CO_2 flux variations south of the STZ, it is incumbent on us to determine the

Table 4.4: Mean values and regression and correlation coefficients of the mean anomaly time series with the SAM index from the pre-industrial run. Regression coefficients correspond to one standard deviation change in the SAM index. Positive air-sea CO₂ flux and vertical velocity correspond to outgassing and upwelling, respectively. Velocities were calculated for the mixed layer.

Zone	Mean Value	Regression	Correlation
<i>Air-sea CO₂ Flux [mol m⁻² yr⁻¹]</i>			
AZ	0.95	0.14	0.56
PFZ	0.78	0.13	0.42
SAZ	-0.68	0.05	0.23
STZ	-0.99	0.02	0.13
<i>pCO₂^{oc} [μatm]</i>			
AZ	294	0.79	0.26
PFZ	280	0.80	0.30
SAZ	268	0.45	0.21
STZ	268	0.09	0.05
<i>Surface sDIC [mmol m⁻³]</i>			
AZ	2166	0.59	0.36
PFZ	2112	0.81	0.32
SAZ	2061	0.36	0.16
STZ	2002	-0.49	-0.20
<i>Mixed Layer Depth [m]</i>			
AZ	60.76	0.95	0.28
PFZ	96.52	1.97	0.30
SAZ	82.92	0.69	0.09
STZ	95.83	-3.05	-0.27
<i>Vertical Velocity [cm s⁻¹]</i>			
AZ	6.2×10^{-5}	1.0×10^{-5}	0.83
PFZ	2.5×10^{-5}	-0.9×10^{-5}	-0.50
SAZ	-2.6×10^{-5}	-1.2×10^{-5}	-0.70
STZ	-5.3×10^{-5}	-0.7×10^{-6}	-0.45
<i>Northward Meridional Velocity [cm s⁻¹]</i>			
AZ	0.37	0.16	0.85
PFZ	0.95	0.14	0.76
SAZ	1.02	0.02	0.14
STZ	0.91	-0.11	-0.59

Table 4.5: Regression coefficients of the SAM index with anomaly time series of the estimated contributions to the $sDIC$ tendency in the region south of the SSTF, integrated over the mixed layer, as in Equation 4.4 [PgC yr $^{-1}$].

Quantity	Natural	Anthropogenic
$\frac{d(sDIC')}{dt}$	0.25	-0.03
$-J'_{ex}$	-0.09	0.02
$-J'_{bio}$	0.03	0
J'_{circ}	0.31	-0.04

mechanisms controlling $sDIC$ anomalies. To accomplish this, we examine the sources and sinks of the modeled tendency in $sDIC$ anomalies,

$$\frac{d(sDIC')}{dt} = J'_{circ} - J'_{bio} - J'_{ex}, \quad (4.4)$$

where J'_{circ} , J'_{bio} , and J'_{ex} represent the sources and sinks of $sDIC'$ from circulation, biology, and CO₂ flux anomalies. J'_{ex} is the anomaly in modeled air-sea flux of CO₂ divided by the depth of the mixed layer. J'_{bio} represents the sink of $sDIC'$ due to organic and calcium carbonate production (see Appendix B for additional details). The circulation term, J'_{circ} is computed by difference. All source and sink terms were calculated for the region south of the SSTF ($\sim 42^\circ\text{S}$), integrated over the annual-mean mixed layer.

We report the results of the $sDIC$ tendency components in (4.4) as regressions of the anomaly time series with the SAM index (Table 4.5). The source of $sDIC$ due to circulation dominates the $sDIC$ anomaly during positive SAM, with the sinks of natural CO₂ outgassing and biology playing smaller roles. This

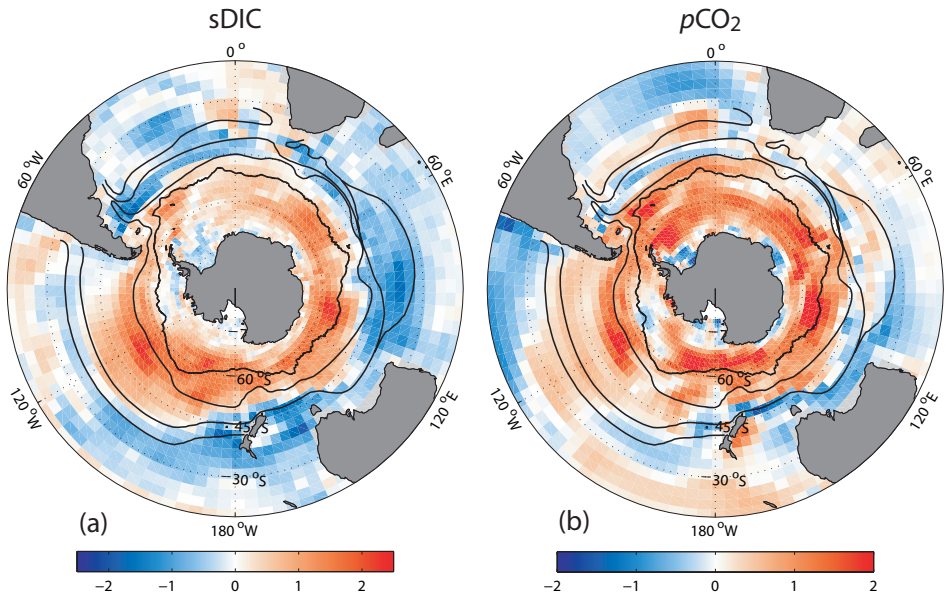


Figure 4.10: Regression of (a) salinity-normalized surface $sDIC$ anomalies (mmol m^{-3}), and (b) $p\text{CO}_2^{oc}$ anomalies (μatm) from the pre-industrial simulation onto the standardised SAM index.

anomalous circulation driving the $sDIC$ source is caused by the stronger overturning in the southern-most regions of the Southern Ocean, which results in a 16% increase in upwelling and a 43% increase in northward meridional velocity in the AZ (Figure 4.11, Table 4.4). The upwelling of $sDIC$ -rich waters and their subsequent lateral transport creates positive anomalies in surface $sDIC$ throughout the AZ, PFZ, and SAZ (Figure 4.9b). A separate calculation not shown here indicates that the deepening of the mixed layer during positive SAM (Table 4.4) also has a small effect on the circulation contribution to $sDIC$. Our findings indicate that biological production does not play a particularly important role in controlling surface $sDIC$ anomalies during positive SAM (Table 4.5).

In summary, both windspeed and surface $sDIC$ changes during positive SAM influence the flux of natural CO_2 between the atmosphere and the Southern

Ocean. We have shown that circulation changes contribute to a large fraction of the *sDIC* anomalies. Similar circulation mechanisms are primarily responsible for the anomalous uptake of anthropogenic CO₂ during positive SAM (Table 4.5), when anomalous upwelling and meridional transport expose deep, older waters to higher atmospheric CO₂ levels. Positive phases of the SAM are therefore associated with simultaneous natural CO₂ outgassing and anthropogenic CO₂ uptake anomalies in the Southern Ocean. This suggests that the same circulation mechanisms which currently drive enhanced outgassing of natural CO₂ from the Southern Ocean during positive SAM may also play a role in mitigating this response in the future, as the anomalous uptake of anthropogenic CO₂ during positive SAM rises due to increasing atmospheric CO₂ concentrations.

4.7 Trends in air-sea CO₂ fluxes

Given the responsiveness of air-sea CO₂ fluxes to interannual variations in the SAM, it is worth investigating how the trend in the SAM influences air-sea CO₂ flux. Our results suggest that the observed secular trend in the SAM between 1958 and 2004 toward more positive phases has led to an outgassing trend of natural CO₂ of 0.006 PgC yr⁻² (Figure 4.4), with a total increase in the outgassing flux over the 47 years of 0.3 PgC yr⁻¹. This trend is masked by the increasing rate of uptake of anthropogenic CO₂, which exhibits a linear trend of -0.011 PgC yr⁻², so that the linear contemporary flux trend of -0.005 PgC yr⁻² is still toward a stronger sink (Figure 4.4). Nevertheless, the secular trend in the SAM has led to a reduction in the rate of increase of the net uptake of atmospheric CO₂ by the ocean. If this trend persists into the next decade or century, as suggested by

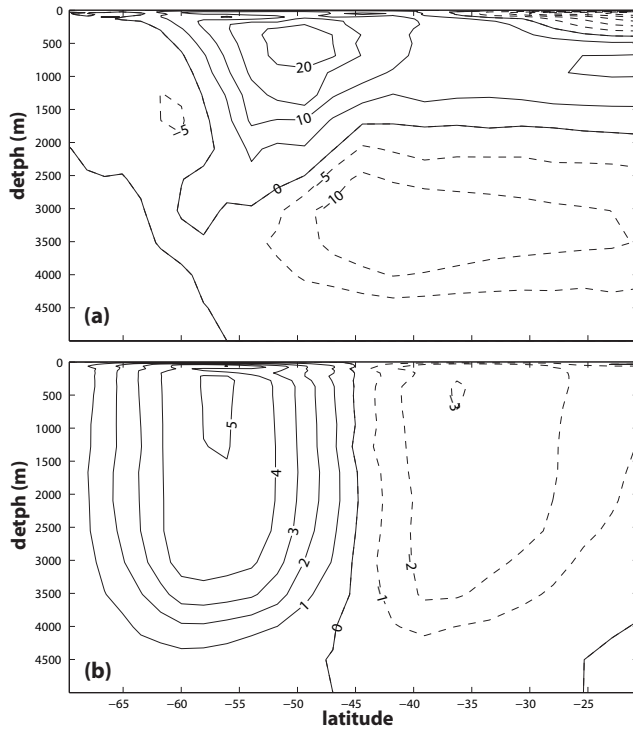


Figure 4.11: (a) Annual-mean meridional overturning streamfunction (Sv), and (b) regression of meridional overturning anomalies from the pre-industrial simulation onto the standardized SAM index, including the Gent and McWilliams (1990) bolus parameterization velocities.

some coupled climate models (see e.g. Fyfe and Saenko (2006)), the associated CO₂ outgassing could cause a positive feedback for the global climate system over this time period.

4.8 Summary

Using a coupled ocean physical-biogeochemical-ecological model, we have demonstrated that the SAM has a significant impact on the flux of CO₂ between the atmosphere and the Southern Ocean under both pre-industrial and historical conditions. During a positive phase of the SAM, we find anomalous outgassing of

natural CO₂ nearly everywhere in the Southern Ocean. The outgassing anomalies are concentrated in the AZ, PFZ, and SAZ, where enhanced overturning brings *sDIC*-rich water to the surface and elevates the $p\text{CO}_2^{oc}$ (Figure 4.9). In contrast, there is a simultaneous anomalous uptake of anthropogenic CO₂ during a positive phase of the SAM in the southern-most regions of the Southern Ocean, due to increased upwelling of deep, older waters and their subsequent exposure to higher atmospheric CO₂ levels. The anthropogenic uptake only slightly mitigates the natural outgassing from the Southern Ocean, so that a positive SAM is associated with anomalous outgassing of contemporary CO₂. In a future characterized by higher atmospheric CO₂, however, positive phases of the SAM may be associated with a greater oceanic uptake of anthropogenic CO₂.

Our findings are supported by a recent study by Butler et al. [submitted manuscript], who investigate the role of the SAM in atmospheric CO₂ concentration variability. They find that positive phases of the SAM are associated with both an elevated rate of increase of atmospheric CO₂ at Palmer Station on the Antarctic Peninsula, and an increase in the flux of CO₂ into the atmosphere from the Southern Ocean. These results inspire confidence in our findings for anomalous outgassing of contemporary CO₂ during positive SAM.

Mounting evidence for a positive trend in the SAM index over the past few decades suggests that the mechanisms we describe here will continue to play an important role in the global carbon cycle over the next century (see Russell et al. (2006)). The impact of future secular trends in the SAM on Southern Ocean air-sea CO₂ flux will compete with climate driven effects, such as increased stratification (e.g. Fung et al. 2005). The mechanisms we describe here may have also

been responsible for past climatic variability. Toggweiler et al. (2006) hypothesize that a feedback exists between the position of the midlatitude westerlies and the atmospheric CO₂ concentrations on paleoclimatic timescales, and that these mechanisms are key for explaining the large CO₂ variations between glacial and interglacial times. Although our simulations cannot test this hypothesis, they do highlight the important role of the Southern Ocean for the global carbon cycle.

Chapter 5

Long-term trends in the Southern Ocean carbon sink

5.1 Abstract

We investigate the long-term trends in the flux of CO₂ between the atmosphere and the Southern Ocean using output from a hindcast simulation of an ocean circulation model with embedded biogeochemistry. We separately investigate trends in the flux of natural, anthropogenic, and contemporary CO₂ by running the model under both pre-industrial and historical atmospheric CO₂ concentrations from 1958 to 2004. We find an outgassing trend of natural CO₂ of 0.006 PgC yr⁻², of which 48% is congruent with the trend in the Southern Annular Mode (SAM). Anthropogenic CO₂ exhibits a trend of -0.011 PgC yr⁻², primarily as a consequence of the anthropogenic perturbation in atmospheric CO₂. The negative trend in anthropogenic CO₂ overwhelms the positive trend in natural CO₂, such that the contemporary CO₂ trend is toward a larger sink over the 47 years.

5.2 Introduction

Many aspects of the Southern Hemisphere climate have exhibited trends over the past few decades. Thompson et al. (2000) observed a 30-year positive trend in the strength of the westerly winds at subpolar latitudes (see, e.g. Figure 5.1a). A trend toward warming on the Antarctic Peninsula and cooling on the interior of the continent has also been observed over this time period (Thompson and Solomon 2002). Additionally, observations of sea ice cover point toward positive trends in the Ross Sea sector and negative trends in the Bellingshausen/Amundsen sector (see, e.g. Figure 5.1b; Parkinson 2004). It has been suggested by Thompson and Solomon (2002) and others that a large fraction of these seemingly heterogeneous trends is closely linked to the positive trend in the Southern Annular Mode (SAM).

A positive trend in the SAM (see, e.g. Figure 5.2) is characterized by a trend toward falling atmospheric pressure over the pole and rising pressure over the mid-latitudes of the Southern Hemisphere (Thompson et al. 2000). This corresponds to a positive trend in the strength of the atmospheric westerlies at $\sim 55^{\circ}\text{S}$, and could therefore cause trends in the circulation and biogeochemistry of the Southern Ocean.

In the previous chapter, we established a strong connection between variability in the SAM and variability in the air-sea flux of CO_2 . Through changes in the wind stress, circulation, and ocean $p\text{CO}_2$, we found that positive phases of the SAM were associated with anomalous outgassing of CO_2 from the Southern Ocean. It follows, then, that a trend toward positive phases of the SAM could be

linked to a trend in Southern Ocean CO₂ fluxes. This connection was originally suggested by Wetzel et al. (2005) and briefly discussed in the previous chapter. Here, we extend on the work from Chapter 4 by examining the total trends in the air-sea flux of CO₂ from the Southern Ocean, and establishing an understanding of the mechanisms driving these trends.

5.3 Methods

As in the previous chapter, we use two simulations from the ocean circulation and biogeochemical model (POP/CCSM) to separately investigate the trends in natural, anthropogenic, and contemporary CO₂ fluxes from 1958 to 2004. The setup of the simulations and the analysis of the model output is identical to that described in Chapter 4, with the exception here that neither the SAM index nor the model output has been detrended. As the trend in the SAM has been shown to have a weak seasonality (Thompson et al. 2000), we investigate only year-round trends.

We use the technique outlined in Thompson et al. (2000) to estimate the linear trends, congruence of the trends with the SAM, and the residual trends. Total trends represent the slope of a straight line which exhibits the best fit to the data. The fraction of the trend that is linearly congruent with the SAM is estimated as the regression coefficient of the data with the SAM index multiplied by the linear trend in the SAM index (0.0245 standard deviations per year). The residual trends are then computed by subtracting the congruent trends from the total trends. Significance of trends is calculated as in Santer et al. (2000), whereby the ratio of the estimated trend and its standard error is compared to

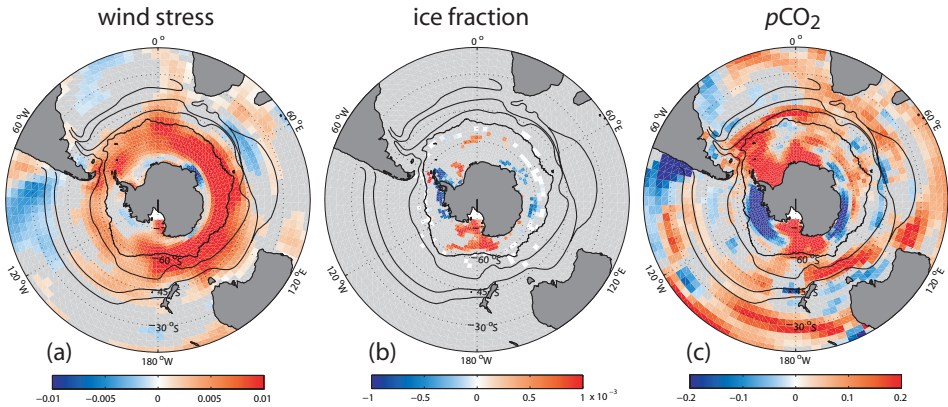


Figure 5.1: Linear trends in (a) wind stress ($\text{dyne cm}^{-2} \text{ yr}^{-1}$), (b) sea ice fraction (yr^{-1}), and (c) ocean $p\text{CO}_2$ ($\mu\text{atm yr}^{-1}$) from 1958 to 2004. $p\text{CO}_2$ trends were calculated for the pre-industrial simulation. Only those trends with significance $\geq 95\%$ are shown.

a t value for a given significance level and effective sample size, while accounting for autocorrelation in the time series (Bretherton et al. 1999).

The skill of this model in representing both the mean state and variability around this mean state was found to be quite reasonable in Chapter 4. However, despite the long spin-up period for these simulations (600 years), we find a globally-integrated ingassing of 0.52 PgC yr^{-1} . This is due to the fact that the model had not yet come into equilibrium with pre-industrial atmospheric CO_2 when the variable forcing was introduced. When correcting for this disequilibrium, we assume that it is spatially uniform. This correction only applies to the mean CO_2 fluxes, and does not impact the trend analysis. The drift is changing at a very slow rate during the 47 years of output that we analyze.

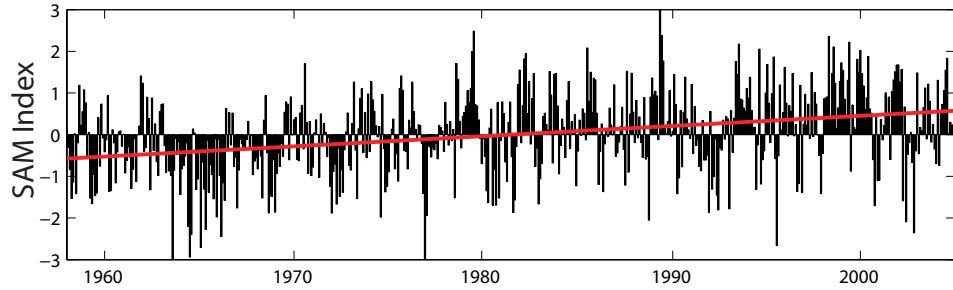


Figure 5.2: Standardized SAM index (black) with linear trend (red) overlain.

5.4 Trends in air-sea CO₂ fluxes

The timeseries of the Southern Ocean (<35°S) integrated air-sea CO₂ fluxes in Figure 5.3 reveals a positive trend for natural CO₂, corresponding to more outgassing with time. The trend has a statistically significant value of 0.0063 PgC yr⁻² (Table 5.1), with a total increase in the outgassing flux over the 47 years of 0.3 PgC yr⁻¹. The spatial pattern of the natural CO₂ flux trend is shown in Figure 5.4a. The trend is positive nearly everywhere, and largest in the southernmost regions of the Southern Ocean.

The flux of anthropogenic CO₂ (Figure 5.3) exhibits a significant negative trend (more oceanic uptake with time) of -0.0114 PgC yr⁻² (Table 5.1), corresponding to a 0.5 PgC yr⁻¹ increase in the uptake rate over the 47 year simulation. The trend is negative nearly everywhere in the Southern Ocean, with parts of the Antarctic Zone (AZ) and the western Atlantic Subantarctic Zone (SAZ) exhibiting stronger trends (Figure 5.4b).

The strong negative trend of anthropogenic CO₂ overwhelms the positive trend of natural CO₂, so that the Southern Ocean flux of contemporary CO₂ exhibits a negative trend of -0.0051 PgC yr⁻² (Figure 5.3, Table 5.1). The sink

strength of anthropogenic CO₂ has greatly increased over the course of our simulation, but the sink strength of natural CO₂ has slightly decreased. The net result is that the Southern Ocean is acting as a stronger sink for contemporary CO₂ at the end of our simulation, as the rate of uptake increases by 0.2 PgC yr⁻¹. The spatial pattern associated with the contemporary trend (Figure 5.4c) reveals that while most of the Southern Ocean exhibits a negative trend, the pattern is by no means spatially coherent, making it difficult to interpret.

5.5 Causes of the trends

In order to understand the mechanisms driving the trend in the air-sea fluxes of CO₂, we must recall that the the natural and anthropogenic components of the total contemporary flux have separate driving factors. Natural CO₂ flux in our model is driven by climate variability and change (through changes in temperature, circulation, and biology), while anthropogenic CO₂ is driven by the increasing atmospheric CO₂, as well as climate variability and change (no role of biology). It is therefore most insightful to investigate the trends of natural and anthropogenic CO₂ separately. We begin with a discussion of the mechanisms driving the natural CO₂ trends, and then study the anthropogenic CO₂ trends before concluding with a short discussion of the total contemporary CO₂ trends.

5.5.1 Natural CO₂

As in the previous chapter, we investigate the mechanisms responsible for the trend in the flux of natural CO₂ by estimating the contributions to the total trend (F') from windspeed (WS), sea ice fraction (Ice), surface DIC , alkalinity

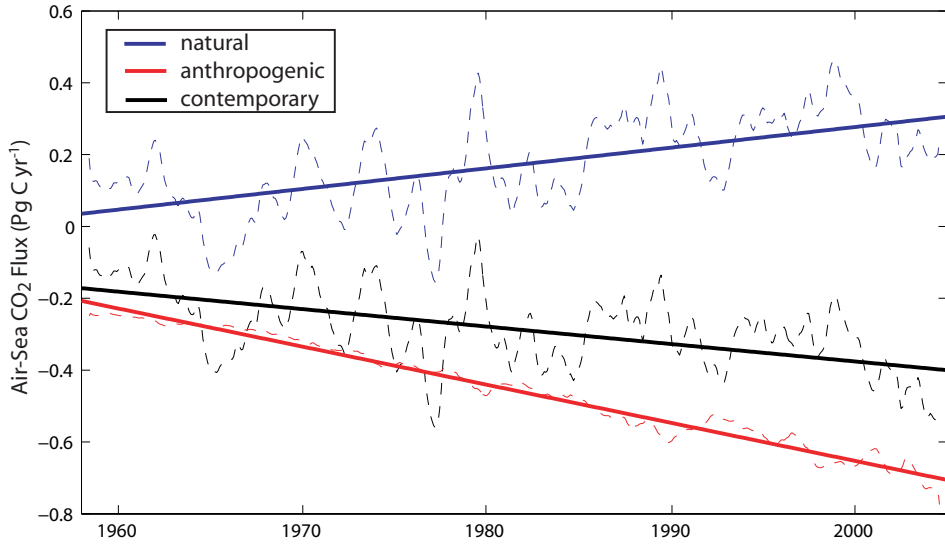


Figure 5.3: Trends in the spatially-integrated Southern Ocean ($<35^{\circ}\text{S}$) fluxes of CO_2 . Smoothed fluxes (12-month running mean) shown as dashed lines for reference. Negative fluxes indicate ocean uptake. Natural and contemporary curves have been adjusted for a global $-0.52 \text{ Pg C yr}^{-1}$ non-equilibrium flux.

(Alk), temperature (T), and salinity (S), while also accounting for changes in DIC and Alk from freshwater fluxes (fw ; see Section 4.6 and Appendix A for additional details). The relative contribution of each parameter to the air-sea CO_2 flux trend in each Southern Ocean region can then be estimated as,

$$\begin{aligned}
F' = & \frac{\partial F}{\partial WS} WS' + \frac{\partial F}{\partial Ice} Ice' + \frac{S}{S_0} \frac{\partial F}{\partial DIC} sDIC' \\
& + \frac{S}{S_0} \frac{\partial F}{\partial Alk} sAlk' + \frac{\partial F}{\partial fw} fw' \\
& + \frac{\partial F}{\partial T} T' + \frac{\partial F}{\partial S} S',
\end{aligned} \tag{5.1}$$

whose individual terms are shown in Table 5.2 and Figure 5.5a.

The analysis of the total trend in natural CO_2 flux demonstrates that all seven terms make important contributions (Table 5.2, Figure 5.5a). The AZ

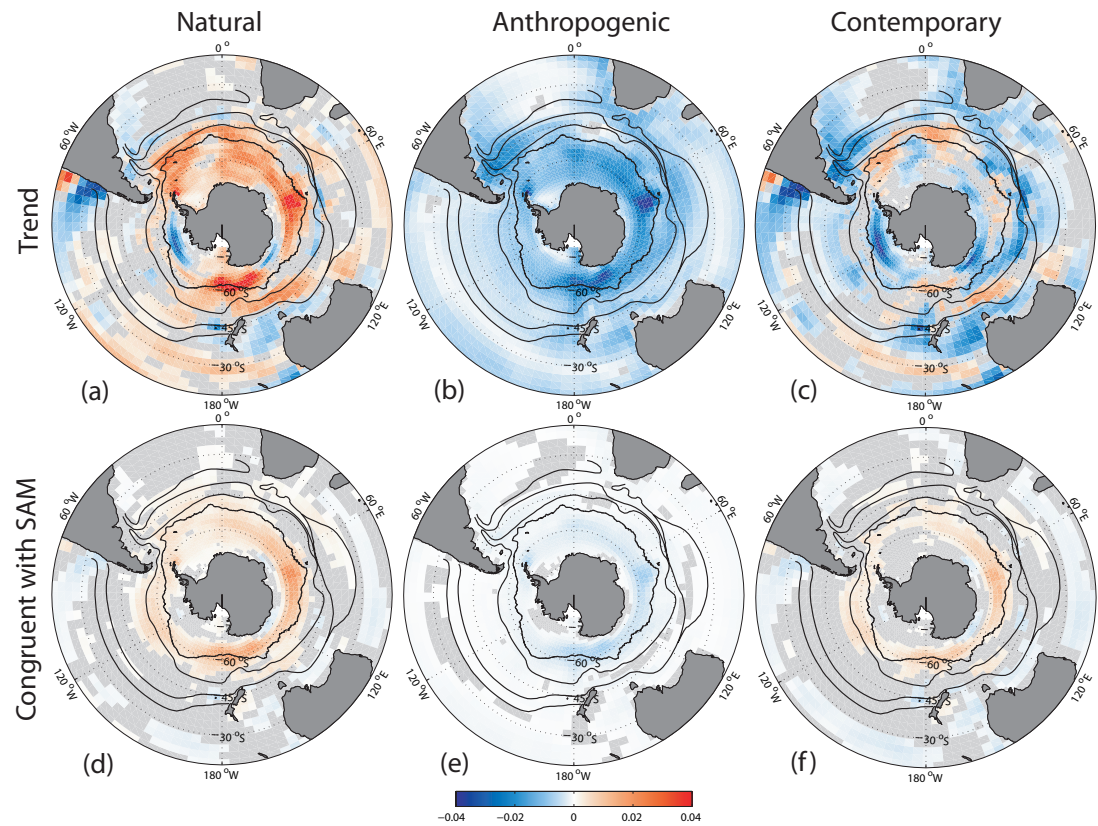


Figure 5.4: (a-c) Linear trends, and (d-f) trends linearly congruent with the SAM in the air-sea flux of (a and d) natural, (b and e) anthropogenic, and (c and f) contemporary CO₂ ($\text{mol m}^{-2} \text{yr}^{-2}$). Only those trends with significance $\geq 95\%$ are shown. Positive values indicate trends toward ocean outgassing.

Table 5.1: Linear trends in the spatially-integrated ($<35^{\circ}\text{S}$) fluxes of CO_2 , and the trends linearly congruent with the SAM (PgC yr^{-2}).

CO_2 Flux	Trend	Congruent with SAM
Natural	0.0063	0.0030
Anthropogenic	-0.0114	-0.0016
Contemporary	-0.0051	0.0014

experiences the largest trend in total flux, where windspeed tends to dominate over a negative contribution from sea-ice, and smaller contributions from the $p\text{CO}_2$ terms ($s\text{DIC}$, $s\text{Alk}$, fw , T , and S). There is a large positive trend in windspeed over the AZ ($30 \text{ cm s}^{-1} \text{ yr}^{-1}$, see, e.g. Figure 5.1a), which explains its large contribution to the trend in natural outgassing. Additionally, the trends in sea-ice and $p\text{CO}_2$, while positive in some portions of the AZ, are negative in other portions (Figure 5.1b and c), resulting in an overall weak contribution for the region. In the Polar Frontal Zone (PFZ), the large trend in outgassing is not overly dominated by any one term, rather all terms except ice make important contributions. The trend in the SAZ is quite small, as the positive contributions from $s\text{DIC}$ and $s\text{Alk}$ are mitigated by a negative windspeed contribution. The trend in the Subtropical Zone (STZ) is negligible, owing to the cancellation of the positive contributions from T and $s\text{Alk}$ by $s\text{DIC}$.

Results from the previous chapter indicate that variability in the SAM explains nearly half of the variance in the air-sea flux of natural CO_2 , suggesting that the positive trend in the SAM could also be linked to the positive trend in the natural CO_2 outgassing from the Southern Ocean. When spatially integrated over the Southern Ocean ($<35^{\circ}\text{S}$), we find that 48% of the trend in the flux of natural CO_2 can be explained by the linear trend in the SAM (Table 5.1). The

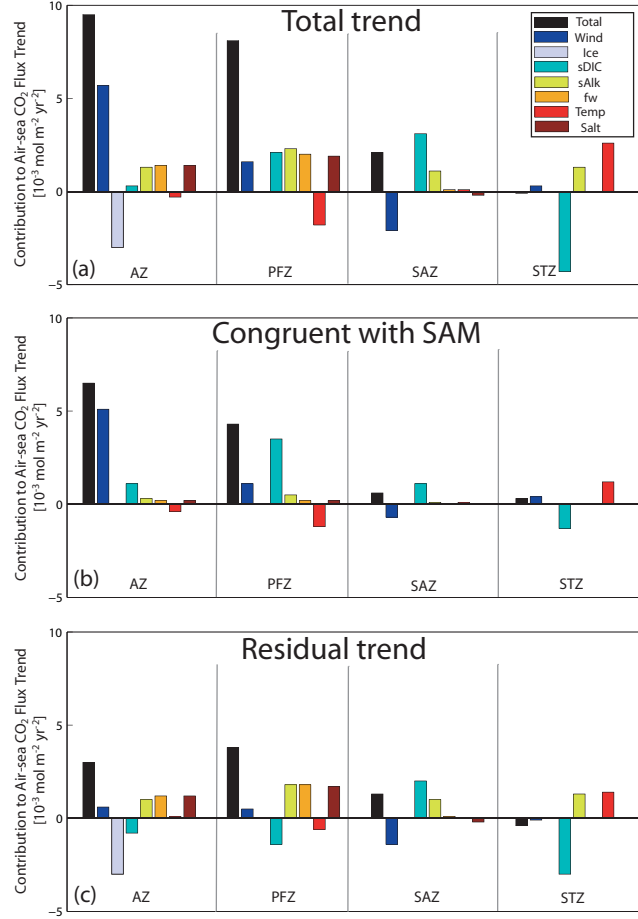


Figure 5.5: Contributions to the trend in natural air-sea CO_2 flux, F' , as in Equation 5.1 ($10^{-3} \text{ mol m}^{-2} \text{ yr}^{-2}$).

spatial congruence of the two is highest in the AZ and PFZ (Figure 5.4d), where more than half of the trend is linearly congruent with the SAM (Figures 5.5a and b).

As a large fraction of the natural CO_2 trend in the Southern Ocean is linearly congruent with the SAM, we investigate in Figure 5.5b the mechanisms which control the fraction of the trend related to the SAM. The methods for this study are identical for those of the total trend, with the exception here that contribu-

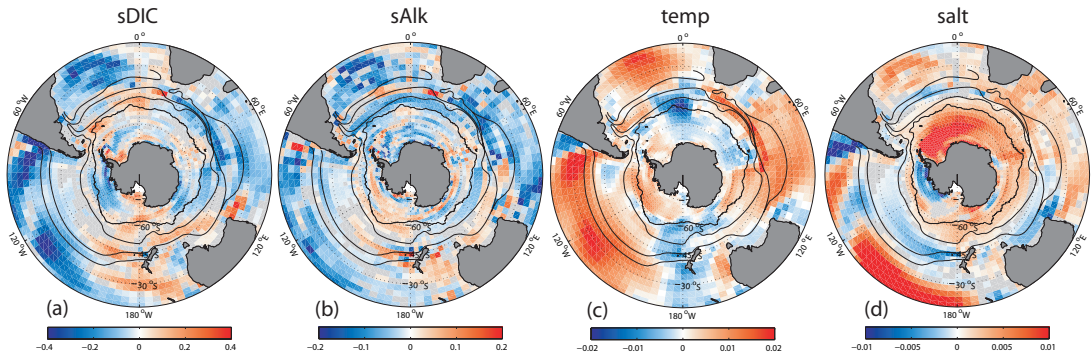


Figure 5.6: Linear trends in surface ocean (a) *sDIC* ($\text{mmol m}^{-3} \text{ yr}^{-1}$), (b) *sAlk* ($\text{mmol m}^{-3} \text{ yr}^{-1}$), (c) temperature ($^{\circ}\text{C yr}^{-1}$), and (d) salinity (psu yr^{-1}) from the pre-industrial simulation. Only those trends with significance $\geq 95\%$ are plotted.

tions from each component are estimated using only the portion that is congruent with the linear trend in the SAM. This analysis reveals that the dominant contributions to the SAM-related trends in CO_2 flux are windspeed and *sDIC*, with opposing contributions from temperature. This agrees with results from the previous chapter, where it was found that windspeed, *sDIC*, and T variations were responsible for CO_2 flux variability in conjunction with the SAM. It follows, then that similar mechanisms, such as trends in upwelling and meridional overturning, are likely responsible for explaining the trend associated with SAM.

While examining the mechanisms controlling the portion of the trend congruent with SAM provides us with some of the explanations behind the total trends, approximately half of the natural CO_2 trend in the Southern Ocean is not linearly congruent with the SAM. This residual portion of the trend was also analyzed as above, and results are shown in Figure 5.5c. Generally, the components contributing to the residual trend are those which did not contribute to the trend in the SAM, namely sea-ice (in the AZ), *sAlk*, fw , and S . Understanding the linear trends in these components is clearly important for explaining the total trend in

natural CO₂ (Figure 5.5a), and yet the patterns associated with the total trends in each of these fields (Figure 5.6) are complex and difficult to interpret. Further work needs to be done in order to understand the mechanisms responsible for these trends.

5.5.2 Anthropogenic CO₂

The primary driver of anthropogenic CO₂ flux in our model is the anthropogenic perturbation in atmospheric CO₂. At the beginning of our simulation (1958), the atmospheric concentration of anthropogenic CO₂ is $\sim 37\mu\text{atm}$, while this value increases to $\sim 100\mu\text{atm}$ by 2004 in a near-linear fashion (not shown). We therefore expect the negative trend in anthropogenic CO₂ uptake to be driven by the positive trend in the atmospheric concentration of anthropogenic CO₂. To check this, we calculate the expected oceanic uptake of anthropogenic CO₂, $F_{expt}^{anth}(t)$, from the flux of anthropogenic CO₂ at the beginning of our simulation, F_o^{anth} , times the ratio of the anthropogenic perturbation in atmospheric CO₂ at a given time, $\chi\text{CO}_2^{anth}(t)$, with the perturbation at the beginning of our simulation, $\chi\text{CO}_{2,o}^{anth}$,

$$F_{expt}^{anth}(t) = F_o^{anth} \times \frac{\chi\text{CO}_2^{anth}(t)}{\chi\text{CO}_{2,o}^{anth}}. \quad (5.2)$$

This technique, used in the oceanic inverse modeling of anthropogenic CO₂ (see, e.g. Gloor et al. 2003; Mikaloff-Fletcher et al. 2006), assumes that the oceanic uptake of CO₂ at any time is linearly proportional to the atmospheric CO₂ perturbation. Further information regarding the technique can be found in the supplementary material from Mikaloff-Fletcher et al. (2006).

Figure 5.7 shows the spatially-integrated ($<35^\circ\text{S}$) values of $F_{expt}^{anth}(t)$ (dashed

Table 5.2: Estimated contributions to the natural air-sea CO₂ flux trends, F' , as in Equation 5.1 [10⁻² mol m⁻² yr⁻²]. Positive fluxes are to the atmosphere. Σ is the sum of all seven terms, and F'_{mod} is the modeled trend in F .

Quantity	AZ	PFZ	SAZ	STZ
<i>Individual Terms</i>				
$\frac{\partial F}{\partial WS} WS'$	0.57	0.16	-0.21	0.03
$\frac{\partial F}{\partial Ice} Ice'$	-0.03	0	0	0
$\frac{S}{S_0} \frac{\partial F}{\partial DIC} sDIC'$	0.03	0.21	0.31	-0.43
$\frac{S}{S_0} \frac{\partial F}{\partial Alk} sAlk'$	0.13	0.23	0.11	0.13
$\frac{\partial F}{\partial fw} fw'$	0.14	0.20	0.01	0
$\frac{\partial F}{\partial T} T'$	-0.03	-0.18	0.01	0.26
$\frac{\partial F}{\partial S} S'$	0.14	0.19	-0.02	0
<i>Sum of Terms Versus Modeled</i>				
Σ	0.95	0.81	0.21	-0.01
F'_{mod}	0.98	0.94	0.43	-0.05

green line), with the linear trend overlain (solid green). A visual comparison of this trend line with that of the actual anthropogenic CO₂ uptake in the Southern Ocean (solid red) indicates that a large fraction (84%) of the linear trend in anthropogenic CO₂ can simply be explained by the linear trend in the anthropogenic perturbation of atmospheric CO₂. The spatial pattern of this expected trend (Figure 5.8a) shows a close correspondence with that of the total anthropogenic trend (Figure 5.4b).

With regard to the portion of the trend (16%) that is not expected from the anthropogenic perturbation in atmospheric CO₂, we examine its spatial pattern in Figure 5.8b. The remaining trend is mostly one of ocean uptake, with the ex-

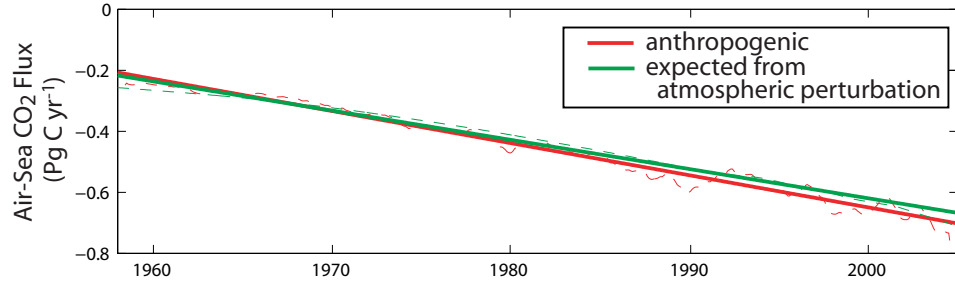


Figure 5.7: Trend in the Southern Ocean ($<35^{\circ}\text{S}$) flux of anthropogenic CO_2 (red), and the trend in anthropogenic CO_2 flux expected from the atmospheric perturbation in anthropogenic CO_2 , as in Equation 5.2 (green). Original time series shown as dashed lines for reference. Negative fluxes imply oceanic uptake.

ception of the Amundsen/Bellingshausen sector and the Atlantic SAZ, where the remaining trend is toward ocean outgassing. In Chapter 4, we demonstrate that $\sim 12\%$ of the variance in anthropogenic CO_2 flux can be explained by the SAM, suggesting that the remaining trend in anthropogenic CO_2 could be connected to the trend in the SAM. We find that 30% of the remaining trend in the region south of 35°S is congruent with the linear trend in the SAM (see Figure 5.8c).

5.6 Implications for the future

Our results indicate that there is a positive trend in the natural CO_2 outgassing over the course of our simulation, and that nearly half of it is congruent with the linear trend in the SAM. Meanwhile, anthropogenic CO_2 has exhibited an ingassing trend over the same period, mostly due to the increasing anthropogenic perturbation in atmospheric CO_2 . The trend in the SAM has therefore led to a reduction in the ability of the Southern Ocean to absorb CO_2 , while the trend in the anthropogenic perturbation of atmospheric CO_2 has led to an increase in the strength of the Southern Ocean carbon sink.

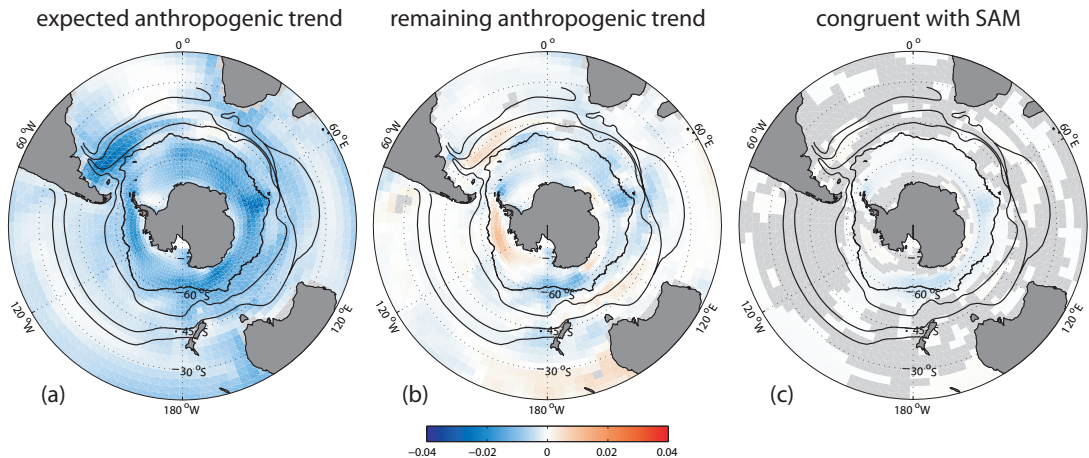


Figure 5.8: Trend in anthropogenic CO₂ flux (a) expected from the atmospheric perturbation in anthropogenic CO₂, (b) remaining trend (total trend in Figure 5.4b minus expected trend), and (c) trend in remaining flux linearly congruent with the SAM (mol m⁻² yr⁻²). Only those trends with significance $\geq 95\%$ are shown. Positive values indicate trends toward ocean outgassing.

In a future characterized by increased greenhouse gas emissions, one would therefore expect the Southern Ocean to act as a much larger sink for anthropogenic CO₂. However, many coupled models (see, e.g. Fyfe and Saenko 2006) are now suggesting that the positive trend in the SAM will continue into the coming century, leading to enhanced outgassing of natural CO₂. It is unknown how these two opposing effects will influence the net carbon sink strength of the Southern Ocean in the future.

5.7 Conclusions

While our simulation exhibits a significant outgassing trend of natural CO₂ from the Southern Ocean, it is masked by a stronger uptake trend of anthropogenic CO₂, so that the trend in Southern Ocean contemporary CO₂ flux is still toward a stronger sink (Figure 5.3, Table 5.1). Seeing as the mechanisms driving both

the natural and anthropogenic CO₂ trends are varying and complex, it is difficult to interpret the spatial pattern of the contemporary trend in Figure 5.4c. The trend in the Southern Annular Mode helps to explain a large fraction of the natural CO₂ flux trend and a smaller fraction of the anthropogenic CO₂ trend. In the absence of the SAM trend, then, the trend in natural CO₂ would likely be reduced, leading to a larger trend in the contemporary sink of atmospheric CO₂.

A comparison of these findings with additional, independent estimates of the trends in the air-sea flux of CO₂ is necessary. Two possible avenues for research on this topic include the use of atmospheric CO₂ inversions and long-term oceanic observations of surface ocean *p*CO₂.

Chapter 6

Summary and conclusions

Using satellite observations and a numerical model, this dissertation investigates the role of the Southern Annular Mode (SAM) in driving variability and trends in the circulation and biogeochemistry of the Southern Ocean on interannual to interdecadal timescales. Through changes in the wind stress, the SAM is shown to have a significant impact on the circulation, biological activity, and carbon cycling in the Southern Ocean.

A large fraction of the variability in the Southern Ocean circulation is found to be linked to the SAM. Observational estimates of surface wind speed indicate that positive phases of the SAM are associated with a poleward contraction of the atmospheric westerlies. This increases the rate of meridional overturning, the amount of upwelling in the Antarctic Divergence, and the northward Ekman transport of waters across the Antarctic Polar Front (APF), as estimated by model output. Observed estimates of surface temperature support these findings, by indicating that a drop in surface temperature is evident to the north of the APF during positive SAM.

Variability in the circulation drives fluctuations in the biological activity, as

evidenced by observations of chlorophyll-*a* concentration. South of the APF, positive phases of the SAM lead to increased chlorophyll, whereas north of the APF, decreased concentrations are found. The response of chlorophyll to SAM variability is likely caused by the interplay between the availability of nutrients and light to fuel production.

The SAM also drives a large fraction of the variability in the flux of CO₂ between the atmosphere and Southern Ocean. Model results suggest that anomalies in the surface concentration of dissolved inorganic carbon via changes in upwelling and northward Ekman transport are the primary cause for these variations. Positive phases of the SAM are found to be associated with an anomalous outgassing of natural CO₂ and a smaller anomalous uptake of anthropogenic CO₂, pointing to an important role for the SAM in controlling global carbon cycle variations.

Model output is used to demonstrate that a large fraction of the trend in the flux of natural CO₂ from the Southern Ocean is related to the positive trend in the SAM. This trend has caused an overall reduction in the strength of the Southern Ocean carbon sink during the past five decades, hinting at a future characterized by reduced sink strength.

Coincident with this dissertation, several other studies suggest that variability in the SAM is causing modifications of Southern Ocean circulation (Ciasto and Thompson, in press; Verdy et al. 2006) and CO₂ fluxes (Butler et al., submitted; Verdy et al., in press; Lenton and Matear, in press), and that feedbacks between the Southern Ocean and atmosphere in association with the SAM could be occurring (Sen Gupta and England, in press; Sen Gupta and England 2006). In conjunction with this work, a consensus is forming on the significance of the

SAM in setting a large portion of the variability in the Southern Hemisphere.

Further research on this topic will need to address some of the issues this study has suffered from, namely the short and sometimes sparse record of satellite chlorophyll, and the resolution and configuration of the ocean model. The community of scientists working with ocean color measurements has shifted from using SeaWiFS observations to those from the Moderate Resolution Imaging Spectroradiometer (MODIS), and while much effort has been made to smooth the transition, the two retrievals of chlorophyll are not necessarily comparable (e.g. Zhang et al. 2006). Estimates of long-term trends in the biota of the Southern Ocean will suffer from this bias. Additionally, it is necessary to bridge the gap between modeled and observed chlorophyll. Despite the complexity of the biogeochemical-ecosystem model used here, significant biases still exist. Neither the mean nor the variability in modeled chlorophyll matches that of the observations, making it difficult to assess the role of the SAM in controlling Southern Ocean biology. The low resolution of the model requires important physical processes, such as eddy transport, to be parameterized rather than represented wholly. This could lead to inconsistencies with reality and cause the model to yield spurious results.

Nevertheless, the insights gained here can be applied toward understanding processes on other timescales. Many coupled climate models are now showing a poleward strengthening of the westerly winds during the next 100 years (see, e.g. Fyfe and Saenko 2006), manifesting itself as a continued positive trend in the SAM index. The cause of this trend is as yet unknown, but the increase of greenhouse gas concentrations and the depletion of stratospheric ozone are both considered

responsible factors (Kushner et al. 2001; Shindell and Schmidt 2004; Arblaster and Meehl 2006; Miller et al. 2006). The SAM will therefore continue to play an important role in the global carbon cycle of the next century. Positive phases of the SAM are associated with anomalous outgassing of CO₂ from the Southern Ocean, and the trend in the SAM over the past five decades has contributed to an outgassing trend of natural CO₂ over this time period. In a future characterized by increased wind stress, then, one could expect an additional amount of natural CO₂ outgassing from the Southern Ocean. If the trend in the SAM is caused by increased greenhouse gas forcing, then the anomalous outgassing of CO₂ could cause a positive feedback in the climate system.

The mechanisms described in this dissertation may have also been responsible for past climatic variability. Toggweiler et al. (2006) hypothesize that a feedback exists between the position of the midlatitude westerlies and the atmospheric CO₂ concentrations on paleoclimatic timescales, and that these mechanisms are key for explaining the large CO₂ variations between glacial and interglacial times.

Shifting winds are only one of the means by which air-sea CO₂ fluxes can feedback on the climate system. For example, there is evidence that the Southern Ocean has become more stratified over the past few centuries (Broecker et al. 1999), and future scenarios suggest that this trend is likely to continue over the next few centuries, due to enhanced poleward transport of tropospheric water vapor and increased precipitation in the high latitudes (Manabe and Stouffer 1993). A more stably-stratified Southern Ocean could potentially alter the upwelling and entrainment of *DIC*-rich waters, resulting in a reduction of natural CO₂ ventilation to the atmosphere (Toggweiler 1999). Conversely, increased stratification

will likely decrease the oceanic uptake of anthropogenic CO₂ (Sarmiento et al. 1998; Caldeira and Duffy 2000). Changes in stratification and wind stress have competing influences on Southern Ocean air-sea CO₂ fluxes, and yet the net effect of these two processes remains unknown.

Past and future estimates of the Southern Ocean carbon sink strength will require the use of numerical and theoretical models, as well as satellite and in-situ observations. It is necessary for the models to more accurately represent the mean state of the Southern Ocean before output from future and past scenarios can be trusted. Satellite observations, while useful in capturing large-scale spatial and temporal variability, are often short-lived records, making it difficult to discern trends in the state of the Southern Ocean. Finally, there is the need for reliable, long-term in-situ observations of both a physical and biogeochemical nature in the Southern Ocean. Such measurements would greatly aid in understanding both short-term variability and long-term trends in the Southern Ocean.

Appendix A

$p\text{CO}_2$ calculations

Anomalous $p\text{CO}_2$ during positive SAM ($\Delta p\text{CO}_2^{oc}$) is decomposed into the contributions from DIC , Alk , T , and S according to (2). To separate the contribution from freshwater fluxes on DIC and Alk , we use the following two equations for the first and second terms of (2),

$$\begin{aligned} \frac{\partial p\text{CO}_2^{oc}}{\partial DIC} \Delta DIC &= \frac{\partial p\text{CO}_2^{oc}}{\partial (S/S_0 \text{ sDIC})} \Delta (S/S_0 \text{ sDIC}) \\ &= \frac{sDIC}{S_0} \frac{\partial p\text{CO}_2^{oc}}{\partial DIC} \Delta S \\ &\quad + \frac{S}{S_0} \frac{\partial p\text{CO}_2^{oc}}{\partial DIC} \Delta sDIC \end{aligned} \quad (\text{A.1})$$

$$\begin{aligned} \frac{\partial p\text{CO}_2^{oc}}{\partial Alk} \Delta Alk &= \frac{\partial p\text{CO}_2^{oc}}{\partial (S/S_0 \text{ sAlk})} \Delta (S/S_0 \text{ sAlk}) \\ &= \frac{sAlk}{S_0} \frac{\partial p\text{CO}_2^{oc}}{\partial Alk} \Delta S \\ &\quad + \frac{S}{S_0} \frac{\partial p\text{CO}_2^{oc}}{\partial Alk} \Delta sAlk. \end{aligned} \quad (\text{A.2})$$

We extract the first terms from (A1) and (A2), as they represent the contri-

bution from freshwater forcing (fw) on $p\text{CO}_2^{oc}$ and account for variability in lateral/vertical circulation working on gradients in salinity,

$$\begin{aligned}\frac{\partial p\text{CO}_2^{oc}}{\partial fw} \Delta fw &= \frac{sDIC}{S_0} \frac{\partial p\text{CO}_2^{oc}}{\partial DIC} \Delta S \\ &+ \frac{sAlk}{S_0} \frac{\partial p\text{CO}_2^{oc}}{\partial Alk} \Delta S.\end{aligned}\quad (\text{A.3})$$

The flux contributions from each region and each process are shown in Table 4.3.

We use the following set of equations to approximate the regional mean values of the $p\text{CO}_2^{oc}$ partial derivatives (Sarmiento and Gruber 2006),

$$\frac{\partial p\text{CO}_2^{oc}}{\partial DIC} = \frac{p\text{CO}_2^{oc}}{DIC} \cdot \gamma_{DIC} \quad (\text{A.4})$$

$$\frac{\partial p\text{CO}_2^{oc}}{\partial Alk} = \frac{p\text{CO}_2^{oc}}{Alk} \cdot \gamma_{Alk} \quad (\text{A.5})$$

$$\frac{\partial p\text{CO}_2^{oc}}{\partial T} \approx p\text{CO}_2^{oc} \cdot 0.0423^\circ C^{-1} \quad (\text{A.6})$$

$$\frac{\partial p\text{CO}_2^{oc}}{\partial S} \approx \frac{p\text{CO}_2^{oc}}{S}, \quad (\text{A.7})$$

where the buffer factors can be approximated with (Sarmiento and Gruber 2006)

$$\gamma_{DIC} \approx \frac{3 \cdot Alk \cdot DIC - 2 \cdot DIC^2}{(2 \cdot DIC - Alk) (Alk - DIC)} \quad (\text{A.8})$$

$$\gamma_{Alk} \approx -\frac{Alk^2}{(2 \cdot DIC - Alk) (Alk - DIC)}. \quad (\text{A.9})$$

Appendix B

Biological fluxes

The biological sink to the *sDIC* anomaly tendency, J'_{bio} , can be defined as

$$J'_{bio} = \frac{\Phi'_{bio}}{h}, \quad (\text{B.1})$$

where h is the depth of the mixed layer and Φ'_{bio} represents the anomalies in the biological flux, defined as the sum of anomalies in the flux of organic carbon and calcium carbonate across the depth of the mixed layer,

$$\Phi'_{bio} = \Phi'_{org} + \Phi'_{CaCO_3}. \quad (\text{B.2})$$

Φ'_{org} is approximated by the anomalous flux of particulate organic carbon, as the anomalous flux of dissolved organic carbon is very small. Substitution of B2 into B1 yields,

$$J'_{bio} = \frac{1}{h}(\Phi'_{org} + \Phi'_{CaCO_3}). \quad (\text{B.3})$$

Bibliography

- Arblaster, J. M. and G. A. Meehl, 2006: Contributions of External Forcings to Southern Annular Mode Trends. *J. Climate*, **19**(12), 2896–2905.
- Banks, H. T., R. A. Wood, J. M. Gregory, T. C. Johns and G. S. Jones, 2000: Are observed decadal changes in intermediate water masses a signature of anthropogenic climate change? *Geophys. Res. Lett.*, **27**(18), 2961–2964.
- Belkin, I. M. and A. L. Gordon, 1996: Southern Ocean fronts from the Greenwich meridian to Tasmania. *J. Geophys. Res.*, **101**(C2), 3675–3696.
- Bousquet, P., P. Peylin, P. Ciais, C. LeQuéré, P. Friedlingstein and P. P. Tans, 2000: Regional Changes in Carbon Dioxide Fluxes of Land and Oceans Since 1980. *Science*, **290**(5495), 1342–1346.
- Boyd, P. W., A. J. Watson, C. S. Law, E. R. Abraham, T. Trull, R. Murdoch, D. C. E. Bakker, A. R. Bowle, K. O. Buesseler, H. Chang, M. Charette, P. Croot, K. Downing, R. Frew, M. Gall, M. Hadfield, J. Hall, M. Harvey, G. Jameson, J. LaRoche, M. Liddicoat, R. Ling, M. T. Maldonado, R. M. McKay, S. Nodder, S. Pickmere, R. Pridmore, S. Rintoul, K. Safi, P. Sutton, R. Strzepek, K. Tanneberger, S. Turner, A. Waite and J. Zeldis, 2000: A mesoscale phytoplankton bloom in the polar Southern Ocean stimulated by iron fertilization. *Nature*, **407**(6805), 695–702.
- Bretherton, C. S., M. Widmann, V. P. Dymnikov, J. M. Wallace and I. Bladé, 1999: The Effective Number of Spatial Degrees of Freedom of a Time-Varying Field. *J. Climate*, **12**(7), 1990–2009.
- Brix, H., N. Gruber and C. D. Keeling, 2004: Interannual variability of the upper ocean carbon cycle at station ALOHA near Hawaii. *Global Biogeochem. Cycles*, **18**, GB4019, doi : 10.1029/2004GB002245.

- Broecker, W. S., S. Sutherland and T.-H. Peng, 1999: A Possible 20th-Century Slowdown of Southern Ocean Deep Water Formation. *Science*, **286**(5442), 1132–1135.
- Butler, A. H., D. W. J. Thompson and K. R. Gurney, submitted: Observed Relationships between the Southern Annular Mode and Atmospheric Carbon Dioxide. *Global Biogeochem. Cycles*.
- Caldeira, K. and P. B. Duffy, 2000: The Role of the Southern Ocean in Uptake and Storage of Anthropogenic Carbon Dioxide. *Science*, **287**, 620–622.
- Campbell, J. W., 1995: The lognormal distribution as a model for bio-optical variability in the sea. *J. Geophys. Res.*, **100**(C7), 13,237–13,254.
- Carleton, A. M., 2003: Atmospheric teleconnections involving the Southern Ocean. *J. Geophys. Res.*, **108**(C4), 8080, doi : 10.1029/2000JC000379.
- Carril, A. F., C. G. Menendez and A. Navarra, 2005: Climate response associated with the Southern Annular Mode in the surroundings of Antarctic Peninsula: A multimodel ensemble analysis. *Geophys. Res. Lett.*, **32**(16), L16713, doi : 10.1029/2005GL023581.
- Cavalieri, D., C. Parkinson, P. Gloerson and H. Zwally, 2002: Sea Ice Concentrations from Nimbus-7 SMMR and DMSP SSM/I Passive Microwave Data. *National Snow and Ice Data Center, Boulder, CO*.
- Ciasto, L. M. and D. W. J. Thompson, in press: Observations of large-scale atmosphere-ocean interaction in the Southern Hemisphere. *J. Climate*.
- Conkright, M. E., H. E. Garcia, T. D. O'Brien, R. A. Locarnini, T. P. Boyer, C. Stephens and J. I. Antonov, 2002: World Ocean Atlas 2001, Volume 4: Nutrients. in S. Levitus, editor, *NOAA Atlas NESDIS 52*, p. 95pp. U.S. Government Printing Office, Washington, D.C., CD-ROMs.
- Doney, S. C., K. Lindsay, I. Fung and J. John, 2006: Natural variability in a stable 1000 year coupled climate-carbon cycle simulation. *J. Climate*, **19**(13), 3033–3054.
- Doney, S. C., S. Yeager, G. Danabasoglu, W. G. Large and J. C. McWilliams, in press: Mechanisms governing interannual variability of upper ocean temperature in a global hindcast simulation. *J. Phys. Oceanogr.*
- Dore, J. E., R. Lukas, D. Sadler and D. M. Karl, 2003: Climate-driven changes to the atmospheric CO₂ sink in the subtropical North Pacific Ocean. *Nature*, **424**, 754–757.

- Fogt, R. L. and D. H. Bromwich, 2006: Decadal Variability of the ENSO Teleconnection to the High-Latitude South Pacific Governed by Coupling with the Southern Annular Mode. *J. Climate*, **19**, 979–997.
- Fung, I., S. C. Doney, K. Lindsay and J. John, 2005: Evolution of carbon sinks in a changing climate. *Proc. Nat. Acad. Sci.*, **102**, 11201–11206, doi : 10.1073/pnas.0504949102.
- Fung, I. Y., S. K. Meyn, I. Tegen, S. C. Doney, J. G. John and J. K. B. Bishop, 2000: Iron supply and demand in the upper ocean. *Global Biogeochem. Cycles*, **14**(1), 281–295.
- Fyfe, J. C. and O. A. Saenko, 2006: Simulated changes in the extratropical Southern Hemisphere winds and currents. *Geophys. Res. Lett.*, **33**, L06701, doi : 10.1029/2005GL025332.
- Garreaud, R. D. and D. S. Battisti, 1999: Interannual (ENSO) and Interdecadal (ENSO-like) Variability in the Southern Hemisphere Tropospheric Circulation. *J. Climate*, **12**(7), 2113–2123.
- Gassó, S. and A. F. Stein, 2007: Does dust from Patagonia reach the sub-Antarctic Atlantic Ocean? *Geophys. Res. Lett.*, **34**(L01801), doi : 10.1029/2006GL027693.
- Gent, P. R. and J. C. McWilliams, 1990: Isopycnal mixing in ocean circulation models. *J. Phys. Oceanogr.*, **20**(1), 150–155.
- Gloor, M., N. Gruber, J. Sarmiento, C. L. Sabine, R. A. Feely and C. Rödenbeck, 2003: A first estimate of present and preindustrial air-sea CO₂ flux patterns based on ocean interior carbon measurements and models. *Geophys. Res. Lett.*, **30**(1), doi : 10.1029/2002GL015594.
- Gordon, A. L., 2001: Interocean Exchange. in G. Siedler, J. Church and J. Gould, editors, *Ocean Circulation and Climate*, pp. 303–314. Academic Press, San Diego, CA, USA.
- Gruber, N., P. Friedlingstein, C. B. Field, R. Valentini, M. Heimann, J. E. Richey, P. Romero-Lankao, D. Schulze and C.-T. A. Chen, 2004: The vulnerability of the carbon cycle in the 21st century: An assessment of carbon-climate-human interactions. in C. B. Field and M. R. Raupach, editors, *The Global Carbon Cycle: Integrating Humans, Climate, and the Natural World*, pp. 45–76. Island Press, Washington, D.C.

- Gruber, N., M. Gloor, S. E. Mikaloff-Fletcher, S. C. Doney, S. Dutkiewicz, M. Follows, M. Gerber, A. R. Jacobson, F. Joos, K. Lindsay, D. Menemenlis, A. Mouchet, J. L. Sarmiento and T. Takahashi, submitted: Oceanic sources and sinks of atmospheric CO₂. *Global Biogeochem. Cycles*.
- Gruber, N., C. D. Keeling and N. R. Bates, 2002: Interannual Variability in the North Atlantic Ocean Carbon Sink. *Science*, **298**, 2374–2378.
- Hall, A. and M. Visbeck, 2002: Synchronous Variability in the Southern Hemisphere Atmosphere, Sea Ice, and Ocean Resulting from the Annular Mode. *J. Climate*, **15**(21), 3043–3057.
- Hartmann, D. L. and F. Lo, 1998: Wave-Driven Zonal Flow Vacillation in the Southern Hemisphere. *J. Atmos. Sci.*, **55**(8), 1303–1315.
- Hughes, C. W., P. I. Woodworth, M. P. Meredith, V. Stepanov, T. Whitworth and A. R. Pyne, 2003: Coherence of Antarctic sea levels, Southern Hemisphere Annular Mode, and flow through Drake Passage. *Geophys. Res. Lett.*, **30**(9), 1464–1467.
- Joos, F., G.-K. Plattner, T. F. Stocker, O. Marchal and A. Schmittner, 1999: Global warming and marine carbon cycle feedbacks on future atmospheric CO₂. *Science*, **284**, 464–467.
- Kalnay, E., M. Kanamitsu, R. Kistler, W. Collins, D. Deaven, L. Gandin, M. Iredell, S. Saha, G. White, J. Woollen, Y. Zhu, M. Chelliah, W. Ebisuzaki, W. Higgins, J. Janowiak, K. C. Mo, C. Ropelewski, J. Wank, A. Leetmaa, R. Reynolds, R. Jenne and D. Joseph, 1996: The NCEP/NCAR 40-Year Reanalysis Project. *Bull. Am. Meterol. Soc.*, **77**(3), 437–470.
- Kara, A. B., P. A. Rochford and H. E. Hurlbert, 2003: Mixed layer depth variability over the global ocean. *J. Geophys. Res.*, **108**(C3).
- Karsten, R. H. and J. Marshall, 2002: Constructing the residual circulation of the ACC from observations. *J. Phys. Oceanogr.*, **32**(12), 3315–3327.
- Keeling, C. D., H. Brix and N. Gruber, 2004: Seasonal and long-term dynamics of the upper ocean carbon cycle at Station ALOHA near Hawaii. *Global Biogeochem. Cycles*, **18**, GB4006, doi : 10.1029/2004GB002227.
- Kidson, J. W., 1999: Principal Modes of Southern Hemisphere Low-Frequency Variability Obtained from NCEP-NCAR Reanalyses. *J. Climate*, **12**(9), 2808–2830.

- Kidson, J. W. and J. A. Renwick, 2002: The Southern Hemisphere Evolution of ENSO during 1981-99. *J. Climate*, **15**, 847–863.
- Kushner, P. J., I. M. Held and T. L. Delworth, 2001: Southern Hemisphere Atmospheric Circulation Response to Global Warming. *J. Climate*, **14**(10), 2238–2249.
- Kwok, R. and J. C. Comiso, 2002: Southern Ocean Climate and Sea Ice Anomalies Associated with the Southern Oscillation. *J. Climate*, **15**, 487–501.
- Large, W. and S. G. Yeager, 2004: Diurnal to decadal global forcing for ocean and sea-ice models: The datasets and flux climatologies. *NCAR Technical Note*, (NCAR/TN-460 STR), 105 pp.
- Lefebvre, W., H. Goosse, R. Timmermann and T. Fichefet, 2004: Influence of the Southern Annular Mode on the sea ice-ocean system. *J. Geophys. Res.*, **109**(C9), 1–12.
- Lefévre, N., A. J. Watson, A. Olsen, A. F. Ríos, F. F. Pérez and T. Johannessen, 2004: A decrease in the sink for atmospheric CO₂ in the North Atlantic. *Geophys. Res. Lett.*, **31**, L07306, doi : 10.1029/2003GL018957.
- Lenton, A. and R. Matear, in press: Role of the Southern Annular Mode (SAM) in Southern Ocean CO₂ uptake. *Global Biogeochem. Cycles*, doi : 10.1029/2006GB002714.
- LeQuéré, C., J. C. Orr, P. Monfray and O. Aumont, 2000: Interannual variability of the oceanic sink of CO₂ from 1979 through 1997. *Global Biogeochem. Cycles*, **14**(4), 1247–1265.
- L'Heureux, M. L. and D. W. J. Thompson, 2006: Observed Relationships between the El Niño-Southern Oscillation and the Extratropical Zonal-Mean Circulation. *J. Climate*, **19**, 276–286.
- Limpasuvan, V. and D. L. Hartmann, 1999: Eddies and the annular modes of climate variability. *Geophys. Res. Lett.*, **26**(20), 3133–3136.
- Liu, J., J. A. Curry and D. G. Martinson, 2004: Interpretation of recent Antarctic sea ice variability. *Geophys. Res. Lett.*, **31**(2), 1–4.
- Liu, J., X. Yuan, D. Rind and D. G. Martinson, 2002: Mechanism study of the ENSO and southern high latitude climate teleconnections. *Geophys. Res. Lett.*, **29**(14), doi : 10.1029/2002GL015143.

- Lovenduski, N. S. and N. Gruber, 2005: Impact of the Southern Annular Mode on Southern Ocean circulation and biology. *Geophys. Res. Lett.*, **32**(11), L11603, doi : 10.1029/2005GL022727.
- Mahowald, N., C. Luo, J. del Corral and C. S. Zender, 2003: Interannual variability in atmospheric mineral aerosols from a 22-year model simulation and observational data. *J. Geophys. Res.*, **108**(D12), 4352, doi : 10.1029/2002JD002821.
- Manabe, S. and R. J. Stouffer, 1993: Century-scale effects of increased atmospheric CO₂ on the ocean-atmosphere system. *Nature*, **364**, 215–218.
- Matear, R. J. and A. C. Hirst, 1999: Climate change feedback on the future oceanic CO₂ uptake. *Tellus*, **51B**, 722–733.
- McCartney, M. S., 1982: The subtropical recirculation of Mode Waters. *J. Mar. Res.*, **40**(suppl.), 427–464.
- McKinley, G. A., M. J. Follows and J. Marshall, 2004: Mechanisms of air-sea CO₂ flux variability in the equatorial Pacific and the North Atlantic. *Global Biogeochem. Cycles*, **18**(2), GB2011, doi : 10.1029/2003GB002179.
- McPhaden, M. J., S. E. Zebiak and M. H. Glantz, 2006: ENSO as an Integrating Concept in Earth Science. *Science*, **314**(1740), doi : 10.1126/science.1132588.
- Mikaloff-Fletcher, S. E., N. Gruber, A. R. Jacobson, S. C. Doney, S. Dutkiewicz, M. Gerber, M. Follows, F. Joos, K. Lindsay, D. Menemenlis, A. Mouchet, S. A. Muller and J. L. Sarmiento, 2006: Inverse estimates of anthropogenic CO₂ uptake, transport, and storage by the ocean. *Global Biogeochem. Cycles*, **20**, GB2002, doi : 10.1029/2005GB002530.
- Mikaloff-Fletcher, S. E., N. Gruber, A. R. Jacobson, M. Gloo, S. C. Doney, S. Dutkiewicz, M. Gerber, M. Follows, F. Joos, K. Lindsay, D. Menemenlis, A. Mouchet, S. A. Muller and J. L. Sarmiento, 2007: Inverse estimates of the oceanic sources and sinks of natural CO₂ and the implied oceanic carbon transport. *Global Biogeochem. Cycles*, **21**, GB1010, doi : 10.1029/2006GB002751.
- Miller, R. L., G. A. Schmidt and D. T. Shindell, 2006: Forced annular variations in the 20th century Intergovernmental Panel on Climate Change Fourth Assessment Report models. *J. Geophys. Res.*, **111**, D18101, doi : 10.1029/2005JD006323.
- Mo, K. C. and M. Ghil, 1987: Statistics and dynamics of persistent anomalies. *J. Atmos. Sci.*, **44**, 877–901.

- Mo, K. C. and R. W. Higgins, 1998: The Pacific-South American modes and tropical convection during the Southern Hemisphere winter. *Mon. Weather Rev.*, **126**, 1581–1596.
- Moore, J. K. and M. R. Abbott, 2000: Phytoplankton chlorophyll distributions and primary production in the Southern Ocean. *J. Geophys. Res.*, **105**(12), 28709–28722.
- Moore, J. K., M. R. Abbott and J. G. Richman, 1999: Location and dynamics of the Antarctic Polar Front from satellite sea surface temperature data. *J. Geophys. Res.*, **104**(C2), 3059–3073.
- Moore, J. K., S. C. Doney and K. Lindsay, 2004: Upper ocean ecosystem dynamics and iron cycling in a global 3-D model. *Global Biogeochem. Cycles*, **18**(4), GB4028, doi : 10.1029/2004GB002220.
- Moore, J. K., S. C. Doney, K. Lindsay, N. Mahowald and A. F. Michaels, 2006: Nitrogen fixation amplifies the ocean biogeochemical response to decadal timescale variations in mineral dust deposition. *Tellus*, **58B**, 560–572.
- Murnane, R. J., J. L. Sarmiento and C. LeQuéré, 1999: Spatial distribution of air-sea CO₂ fluxes and the interhemispheric transport of carbon by the oceans. *Global Biogeochem. Cycles*, **13**(2), 287–305.
- North, G. R., T. L. Bell, R. F. Cahalan and F. J. Moeng, 1982: Sampling errors in the estimation of empirical orthogonal functions. *Mon. Wea. Rev.*, **110**, 699–706.
- Oke, P. R. and M. H. England, 2004: Oceanic Response to Changes in the Latitude of the Southern Hemisphere Subpolar Westerly Winds. *J. Climate*, **17**(5), 1040–1054.
- Parkinson, C. L., 2004: Southern Ocean sea ice and its wider linkages: insights revealed from models and observations. *Antarctic Sci.*, **16**(4), 387–400.
- Peylin, P., P. Bousquet, C. LeQuéré, S. Sitch, P. Friedlingstein, G. McKinley, N. Gruber, P. Rayner and P. Ciais, 2005: Multiple constraints on regional CO₂ flux variations over land and oceans. *Global Biogeochem. Cycles*, **20**, GB1011, doi : 10.1029/2003GB002214.
- Plattner, G.-K., F. Joos, T. F. Stocker and O. Marchal, 2001: Feedback mechanisms and sensitivities of ocean carbon uptake under global warming. *Tellus*, **53B**, 564–592.

- Pollard, R. T., M. I. Lucas and J. F. Read, 2002: Physical controls on biogeochemical zonation in the Southern Ocean. *Deep-Sea Res. II*, **49**(16), 3289–3305.
- Rintoul, S. R., C. W. Hughes and D. Olbers, 2001: The Antarctic Circumpolar Current System. in G. Siedler, J. Church and J. Gould, editors, *Ocean Circulation and Climate*, pp. 271–302. Academic Press, San Diego, CA, USA.
- Robinson, W. A., 2002: On the midlatitude thermal response to tropical warmth. *Geophys. Res. Lett.*, **29**(8), doi : 10.1029/2001GL014158.
- Russell, J. L., K. W. Dixon, A. Gnanadesikan, R. J. Stouffer and J. R. Toggweiler, 2006: The Southern Hemisphere Westerlies in a Warming World: Propping Open the Door to the Deep Ocean. *J. Climate*, **19**(24), 6382–6390.
- Sabine, C. L., R. A. Feely, N. Gruber, R. M. Key, K. Lee, J. L. Bullister, R. Wanninkhof, C. S. Wong, D. W. R. Wallace, B. Tilbrook, F. J. Millero, T.-H. Peng, A. Kozyr, T. Ono and A. F. Rios, 2004: The Oceanic Sink for Anthropogenic CO₂. *Science*, **305**(5682), 367–371.
- Santer, B. D., T. M. L. Wigley, J. S. Boyle, D. J. Gaffen, J. J. Hnilo, D. Nychka, D. E. Parker and K. E. Taylor, 2000: Statistical significance of trends and trend differences in layer-average atmospheric temperature time series. *J. Geophys. Res.*, **105**(D6), 7337–7356.
- Sarmiento, J. L. and N. Gruber, 2006: *Ocean Biogeochemical Dynamics*. Princeton University Press, Princeton, NJ, USA.
- Sarmiento, J. L., N. Gruber, M. A. Brzezinski and J. P. Dunne, 2004: High-latitude controls of thermocline nutrients and low latitude biological productivity. *Nature*, **427**(6969), 56–60.
- Sarmiento, J. L., T. M. C. Hughes, R. J. Stouffer and S. Manabe, 1998: Simulated response of the ocean carbon cycle to anthropogenic climate warming. *Nature*, **393**, 245–249.
- Sarmiento, J. L. and J. R. Toggweiler, 1984: A new model for the role of the oceans in determining atmospheric pCO₂. *Nature*, **308**, 621–624.
- Seager, R., N. Harnik, Y. Kushnir, W. Robinson and J. Miller, 2003: Mechanisms of Hemispherically Symmetric Climate Variability. *J. Climate*, **16**, 2960–2978.
- Sedwick, P. N. and G. R. DiTullio, 1997: Regulation of algal blooms in Antarctic shelf waters by the release of iron from melting sea ice. *Geophys. Res. Lett.*, **24**(20), 2515–2518.

- Sen Gupta, A. and M. H. England, 2006: Coupled Ocean-Atmosphere-Ice Response to variations in the Southern Annular Mode. *J. Climate*, **19**(18), 4457–4486.
- Sen Gupta, A. and M. H. England, in press: Coupled ocean-atmosphere feedback in the Southern Annular Mode. *J. Climate*.
- Shindell, D. T. and G. A. Schmidt, 2004: Southern Hemisphere climate response to ozone changes and greenhouse gas increases. *Geophys. Res. Lett.*, **31**, L18209, doi : 10.10292004GL020724.
- Siegenthaler, U. and T. Wenk, 1984: Rapid atmospheric CO₂ variations and ocean circulation. *Nature*, **308**, 624–626.
- Sigman, D. M., M. A. Altabet, D. C. McCorkle, R. Francois and G. Fischer, 1999: The δ¹⁵N of nitrate in the Southern Ocean: consumption of nitrate in surface waters. *Global Biogeochem. Cycles*, **13**(4), 1149–1166.
- Simmonds, I. and J. C. King, 2004: Global and hemispheric climate variations affecting the Southern Ocean. *Antarctic Sci.*, **16**(4), 401–413.
- Takahashi, T., S. C. Sutherland, R. Wanninkhof, C. Sweeney, R. A. Feely, D. W. Chipman, B. Hales, G. Friederich, F. Chavez, A. Watson, D. C. E. Bakker, U. Schuster, N. Metzl, H. Yoshikawa-Inoue, M. Ishii, T. Midorikawa, C. Sabine, M. Hopema, J. Olafsson, T. S. Arnarson, B. Tilbrook, T. Johannessen, A. Olsen, R. Bellerby, H. J. W. de Baar, Y. Nojiri, C. S. Wong and B. Delille, in preparation: Climatological Mean and Decadal Change in Surface Ocean pCO₂, and Net Sea-air CO₂ Flux over the Global Oceans. *Deep-Sea Res.*
- Thompson, D. W. J. and S. Solomon, 2002: Interpretation of Recent Southern Hemisphere Climate Change. *Science*, **296**(5569), 895–899.
- Thompson, D. W. J. and J. M. Wallace, 2000: Annular Modes in the Extratropical Circulation. Part I: Month-to-Month Variability. *J. Climate*, **13**(5), 1000–1016.
- Thompson, D. W. J., J. M. Wallace and G. C. Hegerl, 2000: Annular Modes in the Extratropical Circulation. Part II: Trends. *J. Climate*, **13**(5), 1018–1036.
- Toggweiler, J. R., 1999: Variation of atmospheric CO₂ by ventilation of the ocean's deepest water. *Paleoceanography*, **14**(5), 571–588.

- Toggweiler, J. R., J. L. Russell and S. R. Carson, 2006: Midlatitude westerlies, atmospheric CO₂, and climate change during the ice ages. *Paleoceanography*, **21**, PA2005, doi : 10.1029/2005PA001154.
- Toggweiler, J. R. and B. Samuels, 1993: New radiocarbon constraints on the upwelling of abyssal water to the ocean's surface. in M. Heimann, editor, *The Global Carbon Cycle*, pp. 333–366. Springer, New York.
- Trenberth, K. E., G. W. Branstator, D. Karoly, A. Kumar, N.-C. Lau and C. Ropelewski, 1998: Progress during TOGA in understanding and modeling global teleconnections associated with tropical sea surface temperatures. *J. Geophys. Res.*, **103**(C7), 14,291–14,324.
- Turner, J., 2004: Review: The El Niño-Southern Oscillation and Antarctica. *Int. J. Climatol.*, **24**, 1–31.
- Verdy, A., S. Dutkiewicz, M. Follows, J. Marshall and A. Czaja, in press: Carbon dioxide and oxygen fluxes in the Southern Ocean: Mechanisms of interannual variability. *Global Biogeochem. Cycles*, doi : 10.1029/2006GB002916.
- Verdy, A., J. Marshall and A. Czaja, 2006: Sea Surface Temperature Variability along the Path of the Antarctic Circumpolar Current. *J. Phys. Oceanogr.*, **36**, 1317–1331.
- Wanninkhof, R., 1992: Relationship between wind speed and gas exchange over the ocean. *J. Geophys. Res.*, **97**, 7373–7382.
- Watson, A. and J. Orr, 2003: Carbon dioxide fluxes in the global ocean. in M. J. R. Fasham, editor, *Ocean biogeochemistry: The role of the ocean carbon cycle in global change*, pp. 123–143. Springer Verlag, Berlin.
- Watterson, I. G., 2000: Southern Midlatitude Zonal Wind Vacillation and Its Interaction with the Ocean in GCM Simulations. *J. Climate*, **13**(3), 562–578.
- Wetzel, P., A. Winguth and E. Maier-Reimer, 2005: Sea-to-air CO₂ flux from 1948 to 2003: A model study. *Global Biogeochem. Cycles*, **19**(2), GB2005, doi : 10.1029/2004GB002339.
- White, W. B. and R. G. Peterson, 1996: An Antarctic circumpolar wave in surface pressure, wind, temperature and sea-ice extent. *Nature*, **380**, 699–702.
- Wilks, D. S., 1995: *Statistical Methods in the Atmospheric Sciences*. Academic Press, San Diego, CA, USA.

- Yeager, S. G., C. A. Shields, W. G. Large and J. J. Hack, 2006: The Low-Resolution CCSM3. *J. Climate*, **19**(11), 2545–2566.
- Yuan, X., 2004: ENSO-related impacts on Antarctic sea ice: a synthesis of phenomenon and mechanisms. *Antarctic Sci.*, **16**(4), 415–425.
- Yuan, X. and D. G. Martinson, 2000: Antarctic sea ice extent variability and its global connectivity. *J. Climate*, **13**, 1697–1717.
- Zhang, C., C. Hu, S. Shang, F. E. Müller-Karger, Y. Li, M. Dai, B. Huang, X. Ning and H. Hong, 2006: Bridging between SeaWiFS and MODIS for continuity of chlorophyll-*a* concentration assessments off Southeastern China. *Rem. Sens. of Environment*, **102**, 250–263.